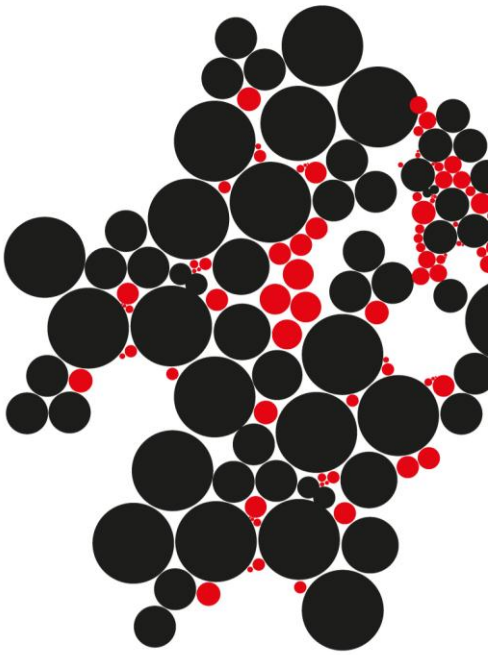

MASTER THESIS

ELECTROHYDRODYNAMIC PROPERTIES OF GOLD SURFACES IN MICRO- AND NANOFLUIDIC STRUCTURES

Worth its weight or superficial glitter?

Marco Verhoog

DEPARMENT OF ELECTRICAL ENGINEERING
BIOS GROUP

EXAMINATION COMMITTEE
Prof.dr. Jan Eijkel
Dr.ing. Egbert van der Wouden
Dr.ir. Wouter Olthuis
Dr.ir. Niels Tas

DOCUMENT NUMBER
2012-14

21-11-2012

UNIVERSITY OF TWENTE.

BIOS Lab on a Chip group

Abstract

This work investigates the influence of gold surfaces micro-and nanofluidic structures. A microfluidic electroosmotic flow pump with an embedded gold surface is manufactured. The fluid flow is characterized with the Current Measurement Method (CCM) and Particle Tracking Velocimetry (PTV). Additionally, a nanofluidic current rectifier with a glass-gold junction is fabricated. The current rectifier is characterized with Impedance Spectroscopy and a theoretical description of the observed phenomena is given. The surface charge of the gold is capacitively controlled, using a novel approach. The gold surfaces in the channels are connected to large gold areas, or “flaps”, outside the channels so that the required potentials to charge these flaps can be dramatically reduced.

Contents

1. Introduction and aim of this work

Suppose you're not feeling well. You try to eat well, sleep well and see if it passes. If it does not, you will probably go see a doctor. You will be questioned, examined and maybe some of your blood is taken to run a few tests. A couple of days later, your blood work comes back from the lab. It turns out you have an bacterial infection. The doctor gives you antibiotics, you quickly feel better and everything is good again.

You were given an excellent diagnosis and you were cured of your illness. However, that does not mean that the diagnosis cannot be even better. First of all, it could be cheaper. This is especially important as in the Netherlands for instance, health care costs rise faster than income levels. Moreover, the diagnosis could be faster. If you would have had a serious infection in an advanced state, you might not have had the luxury of waiting a couple of days for your blood work to come back. Or, the diagnosis could have been more convenient. Maybe you are not that mobile or there is no doctor nearby and you would rather do the diagnosis at home.

These are among the issues that *lab on a chip* technology tries to tackle. A lab on a chip is exactly that: a laboratory the size of chip. It is easy to see why such a devices would be cheaper, a very small machine requires less material to build and is than a large one. If devices are small and cheap than it becomes possible to have one at home, which adds to its convenience. Moreover, smaller samples can be analyzed faster.

A lab on chip is not merely a downscaled version of existing laboratory, because the world on a micro scale differs from the macroscopic one. To illustrate this point, consider a question you might be asked if you would apply for a job at a major technology firm in Silicon Valley. *You are shrunk to the height of a nickel and your mass is proportionally reduced so as to maintain your original density. You are then thrown into an empty glass blender. The blades will start moving in 60 seconds. What do you do?*[1] People have suggested to jam the blades with their clothes so that the electromotor overheats. A more interesting solution, however, is to simply jump out of the blender. This is possible becomes your weight scales with the third power of your length. Your strength, on the other hand, depends on the surface of the cross section of your muscles and therefore scales with the square of your length. That means that if the big you is able to jump out of a blender, the small you most certainly is too.

This example illustrates that in small systems, surface effects gain in relative importance with respect to volumetric effects. This work treats two systems that take advantage of surface properties, or more specifically surface charge, in micro- and nano scale systems. The first is an electroosmotic flow pump, where the speed and the direction of the flow depends on the surface charge. The second is a fluidic diode or current rectifier, which either blocks or conducts an ionic current, depending on the direction of that current. The direction of the diode depends on the surface charge.

Those devices are especially useful if the surface charge can be electrically controlled. That would allow for a fluid flow pump with a controllable flow speed and direction. Moreover, if the direction of the diode can be controlled, than it can be used as a kind of switch to turn an ionic current on and off. Both devices have already been shown [2][3].

The drawback of those devices is that they are made in glass channels and glass interacts with the liquid inside it. Glass has a surface charge that depends on, among other things, the pH of the liquid. And the other way around, if the surface charge of gold is changed electrically, the surface influences the pH of the liquid [4]. Both problems can be circumvented by using gold surfaces instead of glass ones, as gold is an inert material. The aim of this work can now be summarized as follows:

The aim of this project is to design and manufacture fluidic devices with embedded gold surfaces. Then, to build a setup to study the behavior of electroosmotic flow in microchannels and ionic current rectification in nanochannels. Moreover, it is attempted to find a theoretical description for the observed phenomena.

2. Theory of charged surfaces in micro- and nanofluidics

This chapter discusses the theory of charged surfaces in electroosmotic flow pump and ionic current rectifiers. First, a simple model of the electric double layer at the solid-liquid interface is presented. That model is used the explain electroosmotic flow and ionic current rectification. Subsequently, an electrical equivalent circuit of the system is presented to demonstrate the benefits of a gold surface over a glass surface. Moreover, a method that allows for surface charge control is described. Finally, gold related issue such as hydrophobicity and charge polarization are treated.

2.1 The electrical double layer

The electrical double layer arises at the interface between a charged surface and a liquid. In that case, counterions from the solution in the channels will be attracted to the surface, while at the same time coions will be repelled. This means that there is a region close to wall that has a net charge. That region is called the electrical double layer.

The simplest model to describe the electrical double layer is the Helmholtz model. The model assumes that there is a region close to surface with a constant charge density. The charge in this layer shields the surface charge from the bulk liquid. The thickness of this layer is called the Debye screening length, λ_D. It's a concentration dependent parameter and for a symmetrical electrolyte is given by [5]:

$$\lambda_D = \sqrt{\frac{\epsilon_0 \epsilon_r k_B T}{2 n_0 z^2 e^2}} \tag{1.1}$$

With ϵ_0 the permittivity of vacuum, ϵ_r the relative permittivity, k_B the Boltzmann constant, T the temperature, n_0 the bulk concentration, z the valence of the ion, and e the elementary charge. For some applications, such as electroosmotic flow, its more convenient to consider the potential difference over the double layer then the surface charge. In the Helmholtz model there exists a simple relation between those two quantities:

$$\phi_0 = \frac{\sigma}{\epsilon_0 \epsilon_r} \cdot \lambda_D \tag{1.2}$$

With ϕ_0 the potential over the electrical double layer, or the surface potential, and σ the surface charge density. Furthermore, a double layer capacitance per unit area can be derived by differentiating the surface charge density with respect to potential difference over the double layer.

$$C_{DL} = \frac{\partial \sigma}{\partial \phi_0} = \frac{\epsilon_0 \epsilon_r}{\lambda_D} \tag{1.3}$$

Which is the same as the capacitance of infinite parallel plates spaced by a distance of λ_D. It follows from this equation that the double layer capacitance is independent of the potential drop over that layer. This is, however, not the case and other, more complete theories of the electrical double layer have been derived.

A more sophisticated model is that of Gouy-Chapman-Stern. In this model the electrical double layer is divided in two distinct parts. First, there is a layer of closest approach, or Stern layer. This is the closest the ions can approach the surface due to their finite size. This layer is considered one ion diameter thick with a constant charge density. Similar to the Helmholtz model, the potential drops linearly. Secondly, there is a diffuse double layer. In this layer there is a balance between electrostatic and thermal forces. In the Debye-Hückel approximation limit of small surface potentials where $\phi_0 \ll k_B T/\, ze$, the potential drops exponentially:

$$\phi(x) = \phi_s \cdot e^{-\frac{x}{\lambda_D}} \tag{1.4}$$

With ϕ_s the potential at the Stern plane. The capacitance is now the series combination of the Stern capacitance and the diffuse double layer capacitance, which can be more simply expressed as its inverse [5]:

$$\frac{1}{C_{DL}} = \frac{1}{C_S} + \frac{1}{C_{DDL}} = \frac{x_s}{\epsilon_0 \epsilon_r} + \frac{\lambda_D}{\epsilon_0 \epsilon_r \cdot \cosh(ze\phi_s/\, 2kT)} \tag{1.5}$$

With C_S the Stern capacitance, C_{DDL} the diffuse double layer capacitance and x_S the position of the Stern plane, which at one ion radius distance from the surface. The equivalent capacitance of two capacitors in series is determined by the smallest of the two. It follows from Equation (1.1) that for low electrolyte concentration the Debye length is much larger than the radius of an ion. In that case, the double layer capacitance is largely determined by the diffuse double layer. For low surface potentials, the value of the hyperbolic cosine of (1.5) is close to one, reducing the equation o for the double layer capacitance to Equation (1.3).

Electroosmotic flow pumps and ionic current rectifiers require electrodes to create potentials difference in the solution. These electrodes also have a double layer capacitance. The capacitance is charged when there is a potentials difference between the electrode and the solution. Moreover, if the potential difference exceeds a certain threshold voltage, there will also be a faradaic current between the electrode and the solution due to redox reactions. He threshold voltage depends on the electrode material and the ions in the solution. This phenomenon can modeled as an electrical equivalent circuit with an impedance parallel to capacitor, as shown in Figure 1. The impedance is very high for low voltages over the double layer and low for high voltages. This voltage dependant impedance is called a Warburg impedance.

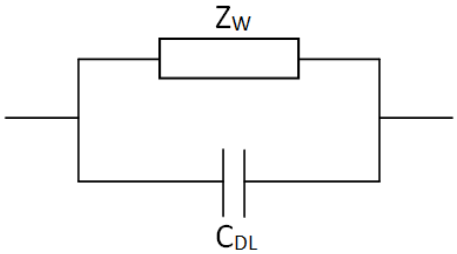

Figure 1: Electrical equivalent circuit of the double layer consisting of an capacitor parallel to the variable Warburg impedance.

2.2 Fluid flow in microchannels

Electroosmotic flow is used as a pumping mechanism in microfluidic systems. Unlike its mechanical counterparts, it does not suffer from downscaling. Mechanical fluid pumps, whether they feed gasoline to your engine or push blood through your veins, usually work by creating an elevated pressure. Then, fluid will flow in the direction of decreasing pressure. The magnitude of that flow is proportional to the pressure difference and inversely proportional to the hydraulic resistance of the system. When systems are downscaled, however, the hydraulic resistance increases with the third power of the channel height reduction. Subsequently, large pressure gradients are necessary, requiring large pumps, which rather defy the purpose of downscaling.

Electroosmotic flow pumps take advantage of the net charge that is present in the electrical double layer. If an electric field is applied parallel to the channel wall, there will be an electrical body force on the ions in the double layer equal to $\rho \cdot E$, with ρ the charge density. These ions, in turn, drag along the rest of the fluid trough friction forces. A steady flow is reached when the electrical forces equal the friction forces. The resulting speed is given by the Helmholtz-Smoluchowski equation:

$$v_{EOF} = \frac{\epsilon_0 \epsilon_r}{\eta} \zeta E \tag{1.6}$$

With η is the viscosity of the fluid and ζ the potential at the slipping plane. This ζ-potential equals φ_0 when the Helmholtz model of the electrical double layer is used as the surface is the slipping plane. However, according to the Gouy-Chapman-Stern theory, the electrostatic forces in the Stern layer are so strong that the ions are rendered immobile. Therefore, the slipping plane is at the boundary of the Stern layer.

Equation (1.6) shows that the magnitude of the electroosmotic flow depends on the electric field, the viscosity of the fluid and the arrangement of ions in the electrical double layer, but is independent of geometry.

Another useful phenomenon that is specific to small channels is capillary pressure. This effect occurs when a liquid has high affinity for the channel walls. In that case it becomes energetically favorable for the liquid to maximize the liquid-surface overlap area, dragging the liquid into the channel. The capillary pressure for a circular channel is given by:

$$p_c = \frac{2\gamma cos\theta}{r} \tag{1.7}$$

With p_c the capillary pressure, γ the surface tension, θ the contact angle and r the effective radius of the channel. The contact angle is a measure of the affinity of the liquid and the surface. For a contact angle smaller than 90°, the capillary pressure will push the liquid into the channel and the surface is called wettable. Capillary forces are often used to fill micro- and nanochannel.

Capillary forces can also cause a pressure difference over an already filled channel. If the shape of the surface at both ends of the channel differs than so will the pressure. The pressure difference over the channel is given by the Yong-Laplace equation:

$$\Delta p = \gamma \left(\frac{1}{R_1} + \frac{1}{R_2} \right) \tag{1.8}$$

With R_1 and R_2 the radii of curvature at the liquid are interface. The radius of curvature depends on the shape of the surface at the interface. Small defects there can lead to significant changes in curvature radius and a large pressure difference.

2.3 Nanofluidic ionic current rectifier

Fluidic diodes, like their better known semiconductor counterparts, have a lower electrical resistance in one direction than in the opposite direction. The current rectification in the fluidic variant is caused by an asymmetry in ion concentrations along the channel. That asymmetry can be created by varying the surface charge along the channel [6][3][7], varying the height of the channel [8] or if the bulk concentrations at both ends differs. To explain the rectifying effect, consider the fluidic channel of Figure 2a. The red bars show the magnitude of the cation concentration at the left, c^+_L, and right, c^+_R, side of the channel. Similarly, the green bars indicate the anion concentrations. The channel is designed such that the cation to anion ratio at the left side of the channel differs from the ratio at the right side of the channel. Now, if an electric field is applied over the channel, there will be an ionic current. When the mobilities of the cations and ions are equal, the current density will be proportional to their respective concentrations. From current continuity we know that the current must be constant along the channel. However, the fraction of current carried by the cations or anions varies throughout the channel. If the electric field is applied from left to right, as depicted in Figure 2b, then the channel is depleted of cations as the influx from the left side is lower than the efflux at the right side. Likewise, the efflux of anions at the left side exceeds the influx from the right, so that they are depleted also. If the direction of the electric field is reversed the opposite occurs and both cations and anions will accumulate in the channel. The current through the channel is proportional to the total amount of ions present. The depleted channel will therefore have a low conductivity and can be said to be reversed biased. When ions accumulate in the channel its conductivity increases and it is in forward bias.

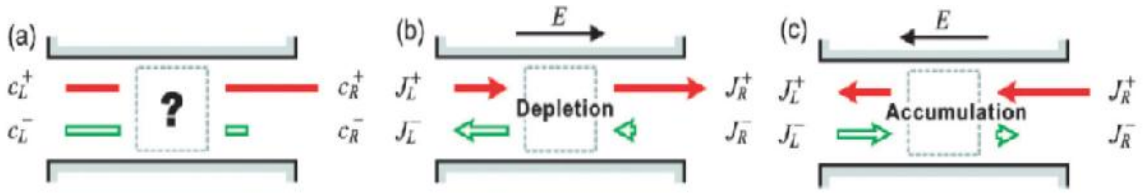

Figure 2: Current rectifying mechanism in a fluidic channel. a) The magnitude of the cation concentrations, c^+, is represented by the length of the red bar and the anion concentration, c^-, by the length of the green bar. The left side of the channel has equal cation and anion concentrations, while the right side has not. Applying an electric field over the trough the channel causes it to b) deplete of ions or c) accumulate ions depending on the direction of that field. [9]

To design a fluidic diode it is necessary to determine the parameters that affect the ion the concentrations. A clear and intuitive approach is to consider the cation to anion ratios, as suggested by Cheng and coworkers [9]. They derive an expression for the cation to anion ratio based on the law of mass action and the assumption of electroneutrality. If electroneutrality in the nanochannel is assumed, then the sum of the fixed charge on the channel walls and the ions in the channels should be zero.

$$c_+ - c_- + f = 0 \tag{1.9}$$

With

$$f = \frac{2\sigma_s \cdot 10^{-3}}{eN_A h} \tag{1.10}$$

Where σ_s is the surface charge density, e the elementary charge, N_A Avogadro's number and h the channel height. Furthermore, the law of mass action states

$$c_+ c_- = c_b^2 \tag{1.11}$$

Where c_b is the bulk concentration. Solving for the cation and anion concentrations yields:

$$c_+ = -\frac{f}{2} + \sqrt{\left(\frac{f}{2}\right)^2 + c_b^2} \tag{1.12}$$

$$c_- = \frac{f}{2} + \sqrt{\left(\frac{f}{2}\right)^2 + c_b^2} \tag{1.13}$$

Defining α as the ratio between the cation and anion concentrations we get:

$$\alpha = \frac{c_+}{c_-} = \frac{-\frac{f}{2} + \sqrt{\left(\frac{f}{2}\right)^2 + c_b^2}}{\frac{f}{2} + \sqrt{\left(\frac{f}{2}\right)^2 + c_b^2}} \tag{1.14}$$

Which can be rewritten as:

$$\alpha = \left(\frac{-f + \sqrt{f^2 + 4c_b^2}}{2c_b} \right)^2 \tag{1.15}$$

From these equations it follows that the ratio of cations to anions can be controlled by varying the bulk concentration, the surface charge density or the geometry along the channel. Furthermore, it can be seen that for $c_b >> f$ the cation concentration equals the anion concentration. Or, put differently, cation and anion concentrations will be equal if the surface charge is much lower than the total charge in the channel.

It is important to consider under which circumstances a rectifying device is most effective. We have seen that the rectifying effect stems from the accumulation and depletion of ions inside the channel. That effect, in turn, is caused by an imbalance in the amount of current carried by cations and anions at the left and right side of the channel. Therefore, it is useful to define a ratio, β, that characterizes that imbalance.

$$\beta^+ = \frac{J_L^+}{J_R^+}, \beta^- = \frac{J_L^-}{J_R^-} \tag{1.16}$$

Where J is the current density, the subscript R and L are used to indicate the left and right side of the channel and + and – indicates cations and anions. Now, from current continuity we know

$$J_L^+ + J_L^- = J_R^+ + J_R^- \tag{1.17}$$

And therefore

$$\beta^+ = \frac{J_L^+}{J_R^+} = \frac{J_R^+}{J_R^+} + \frac{J_R^-}{J_R^+} - \frac{J_L^-}{J_R^+} \tag{1.18}$$

If the cations and anions have the same mobility, then the second term in the equation above is equal to ratio c_R^-/c_R^+ or $1/\alpha_R$. Furthermore, the last term can be rewritten as

$$\frac{J_L^-}{J_R^+} = \frac{J_L^-}{J_R^+} \cdot \frac{J_L^+}{J_L^+} = \frac{J_L^+}{J_R^+} \cdot \frac{J_L^-}{J_L^+} = \beta^+ \cdot \frac{1}{\alpha_L} \tag{1.19}$$

Solving for β^+ gives

$$\beta^+ = \frac{1 + {}^1/_{\alpha_R}}{1 + {}^1/_{\alpha_L}} \tag{1.20}$$

Similarly, we find for β^-

$$\beta^- = \frac{1 + \alpha_R}{1 + \alpha_L} \tag{1.21}$$

Accumulation and depletion effects occur if the cation or anion transport is not constant throughout the channel, that means if either β^+or $\beta^- \neq 1$. If the bulk concentration is high compared to the charge in the double layers we get $\alpha_R \approx \alpha_L \approx 1$ and both β^+ and β^- are approximately 1. In that case, there will not be a rectifying effect. Another special case occurs if each side of the channel has a different surface charge density but of equal sign, let say negative. Now, for low concentrations, $\alpha_L \gg 1$ and $\alpha_R \gg 1$ but $\alpha_L \neq \alpha_R$ and thus $\beta^+ \approx 1$ and $\beta^- \neq 1$. That implies that there will be a change of anion concentration in the channel. However, as the cations are the majority charge carriers, that change is expected to be very limited. In this regime, charge transport is dominated by the counterions in the double layer. This system behaves as series connection of two resistances instead of as a diode.

The cation to anion ratio α and the imbalance ratio β are useful figures to give a qualitative description of the functioning and to obtain an intuitive understanding of the current rectification mechanism. A complete description of the system, however, should also account for the diffusive currents that arise due to concentration differences between the junction and the bulk. These forces counteract the depletion or accumulation at the junction.

The Poisson-Nernst-Planck equations are often used to calculate to combined effect of diffusion and migration current. The Poisson equation relates the potential profile to the charge density.

$$-\nabla\epsilon_0\epsilon_r\nabla V = F\sum_i z_i c_i \tag{1.22}$$

Here, $\epsilon_0$is the permittivity of vacuum, ϵ_r the relative permittivity, V the potential, F the Faraday constant, z_i the valency of ion species i, and c the concentration of species i. The Nernst-Planck equation determines the ion flux due to diffusion and migration.

$$J_i = -(D_i\nabla c_i + z_i\mu_i F c_i\nabla V) \tag{1.23}$$

Where the first term of the equation is the contribution due to diffusion with D is the ion diffusion constant. The second term describes the migration current density, where μ is the ion mobility. For a steady state solution, the charge conservation law gives:

$$\nabla\cdot J_i = 0 \tag{1.24}$$

These 3-dimensional equations or usually simplified to a 1-dimensial problem, where only changes in the direction of the channel are considered. The solutions of these simplified equations are still cumbersome, but can be simplified even further even only large bias voltages are considered. Here, the solutions as presented by Cheng and coworkers in [7] are considered. First, they define fixed charge density *f* as a function of the surface charge density and channel geometry.

$$f = \frac{2\sigma_s}{eN_A h} \tag{1.25}$$

With *e* the elementary charge and N_A Avagadro's number. Next, they split the solutions for large forward biases in a case for low salt concentrations, c≪f/2 and, and for high concentrations, where c≫f/2. At low concentrations:

$$J_F = \left(c_b \ll \frac{f}{2}\right) = DF\frac{f}{2l}\left(\frac{F}{RT}V_d + \frac{1}{4}\left(\frac{F}{RT}V_d\right)^2\right) \tag{1.26}$$

With J_F the current density in forward direction and V_d the potential over the junction. The current density becomes a quadratic function of the junction potential when $V_d > 4\frac{RT}{F} = 100mV$. At high concentrations:

$$J_F = \left(c_b \gg \frac{f}{2}\right) = DF\frac{1}{l}\left(c_b\frac{F}{RT}V_d + \frac{f}{8}\left(\frac{F}{RT}V_d\right)^2\right) \tag{1.27}$$

Now, the current density becomes a quadratic function of the junction potential when $V_d > 8\frac{RT}{F}\frac{c_b}{f} = \frac{c_b}{f}\cdot 200mV$. As the salt concentration is much larger than the fixed charge density there will be linear dependency of the current density for low junction potentials.

$$J_F = \left(c_b \gg \frac{f}{2}\right) = \frac{DF^2}{RTl}(c_b V_d) \tag{1.28}$$

Under large reverse bias, the voltage drop will occur at the channel junction. The current in reverse bias is given by:

$$J_{sat} = (V_d \ll 0) = -\frac{2DF}{fl} c_b^2 \quad (1.29)$$

From the equation it follows that the current in reverse bias is a function of the square of the bulk concentration. Interestingly, the saturation currents seems independent of the junction potential V_d. However, the junction potential is implied in the condition of a large reverse bias. This means that if the junction potential is large enough to the deplete the channel, than the current saturates and it becomes independent of junction potential.

2.4 Surface charge actuation

Electroosmotic pumping in microchannels and current rectification in nanochannels are defined by the charges and potentials at the channel surface. Therefore, control of those surface properties makes it possible to create reconfigurable fluidic circuits. Surface charge control has been shown using an additional electric field, perpendicular to the channel wall. That field will attract more counterions or coions to channel surface. This field effect control of the electroosmotic flow has been shown by Schasfoort and coworkers [2]. More recently, a nanofluidic diode has been shown in a heterogeneous that worked by controlling the surface charge of half the channel [3]. Both of these devices use channels made from an electric insulator and an external gate electrode. The insulator is necessary to ensure that there are no faradaic currents injected into the fluid by the electrode. A schematic overview of such a design is shown in Figure 3.

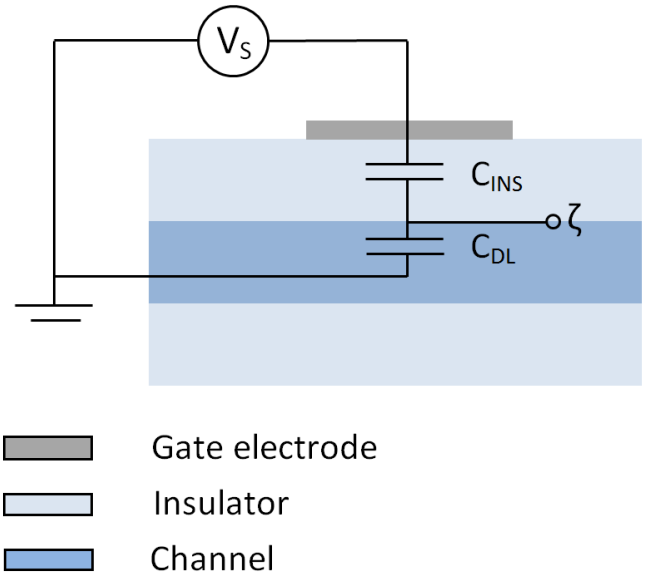

Figure 3: Capacitive model of surface charge actuation in a microfluidic channel.

Electrically, the system of Figure 3 can be modeled as two capacitances in series, where one is the insulator capacitance C_{INS} and the other the double layer capacitance C_{DL}. The gate potential is denoted with V_S and the ζ-potential is also included in the schematic.

The insulator capacitance can be modeled as a parallel plate capacitance, where the gate electrode is one of the plates, the insulator surface at the liquid interface the other plate and the insulator material is the dielectric. The capacitance per unit area is given by:

$$C_{INS} = \frac{\epsilon\epsilon_r}{d} \tag{1.30}$$

With *d* the spacing between the two plates. This equation holds if the spacing is relatively small compared to the surface area of the plates. When the width or the length of one of the plates is of the same order of magnitude as the height, the capacitance deviates significantly from the values found with Equation (1.30)[10]. In Equation (1.3)(1.2), the electrical double layer capacitance is also considered a parallel plate capacitance where the spacing between plates is equal to the Debye screening length λ_D.

If a voltage, V_S, is applied between the electrode and the solution than the change in potential at the solid-liquid interface is given by:

$$\Delta V = \frac{C_{INS}}{C_{INS} + C_{DL}} \cdot V_S \tag{1.31}$$

For cases where the double layer capacitance is much larger than the insulator capacitance the latter can be dropped from the denominator of Equation (1.31). Including the areas of the capacitances in the equation yields:

$$\Delta V = \frac{C_{INS}}{C_{DL}} \cdot \frac{A_{INS}}{A_{DL}} V_S \tag{1.32}$$

With *A* denoting the areas. The change in surface potential due to the application of a gate voltage can be increased by increasing A_{INS} with respect to A_{DL}. This property will be exploited in the design of the fluidic circuits.

Insulators, generally have an additional contribution to the surface charge due to interfacial chemistry. Glass, for instance, has surface silanol groups, which deprotonate when it is in contact with a liquid of neutral pH. This deprotonation changes the surface charge and is usually taken advantage of in EOF pumps as it eliminates the necessity of an extra electrical field to induce surface charges. At the same time it poses two challenges for the precise control of the surface charge. Firstly, the amount of surface deprotonation depends on the pH of the fluid inside the channel. Therefore, the pumping speed varies for different fluids. Secondly, the efficiency of the capacitive surface charge control is decreased due to the buffering capability of the interface. A change of the potential on the gate electrode will either result in a change in surface potential or in (de)protonation of the surface [4]. The former leads to a change of charge in the mobile double layer, while the latter does not. Moreover, (de)protonation leads to an unwanted change in the acidity of the fluid.

The electric equivalent model of Figure 3 can be expanded so that it encompasses these additional terms. The pH depended surface charge is modeled by an additional potential source while the buffering capacity is modeled by a capacitance in series. The expanded model is shown in Figure 4, with C_B the buffer capacitance and V(pH) the pH dependent voltage source.

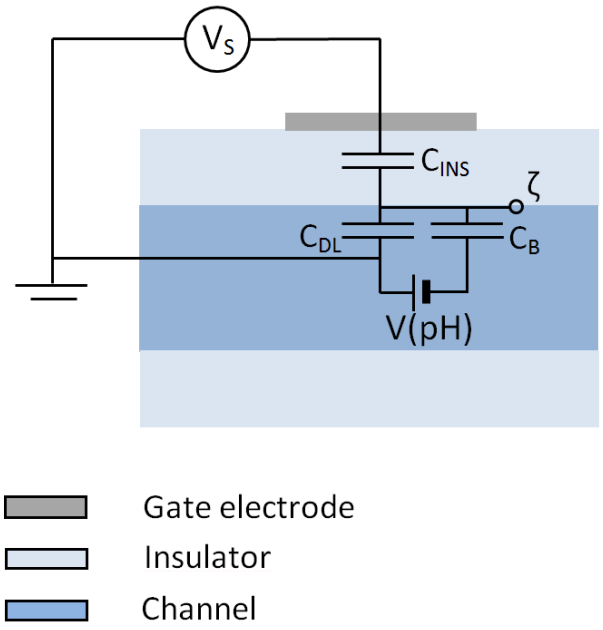

Figure 4: Capacitive model of surface charge actuation in a microfluidic channel including the buffer capacitance of the insulator surface as well as an pH dependent voltage source.

Ideally, the surface charge should be independent of the fluid in the channel and the properties of the fluid should not change due a gate potential. This independence can be accomplished by adding a layer of gold on the channel surface as shown in Figure 5. Gold is chosen as the preferred surface of the microchannels, because it doesn't oxidize easily. Therefore, its surface charge density is highly robust to changes in the pH of the solution. The expression for the change in surface potential reduces to Equation (1.31) again.

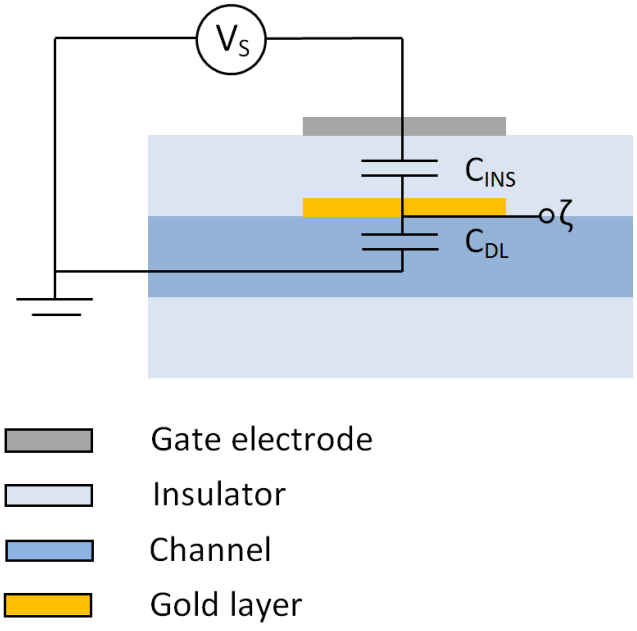

Figure 5: Capacitive model of surface charge actuation in a microfluidic channel with gold surface.

2.5 Charge polarization of floating gold layers

The surface of the channels are coated with a layer of gold. If no current can flow from the solution to the gold or vice versa than the gold is considered to be floating. Now, if a voltage is apllied over the channel, there will also be a potential difference over the gold strip. However, as gold is a very good cunductor, there will immediately be a current inside the gold. As the current has nowhere to go, this means that charge must build up at the edges of the gold. These charges, in turn, create there own electric field, negating the external one so that a steady state is reached. This phenomenom is called the polarization of gold.

An elegant way to examine the behavior of a system with such floating electrodes is by considering the surface potentials [11]. If an electric field is applied over that channel, than the bulk potential will be.

$$\phi_b(x) = \phi_s \cdot \left(1 - \frac{x}{L}\right) \tag{1.33}$$

Where ϕ_b, is the bulk potential, ϕ_s the source potential, x the position along the channel and L the channel length. The electrode, being a very good conductor, must be a equipotential:

$$\phi_g = \phi_s \cdot \left(1 - \frac{x_g}{L}\right) \tag{1.34}$$

Where x_g is the x position of the middle of the gate-electrode. Now, the zeta potential created by the parallel field is:

$$\zeta(x) = \phi_s \cdot \left(1 - \frac{x - x_g}{L}\right) \tag{1.35}$$

As the electroosmotic flow depends on the ζ-potential it is plausible that the gold surface of a channel will affect it. However, as the change in ζ-potential is symmetrical around the middle of the gold electrode, it will not lead to net electroosmotic flow. The local changes in flow speed can lead to turbulence, which might lead to a more subtle influence on the flow.

The effect of gold polarization is much more significant for the current rectifier. The behavior of the diode is examined for three different voltages over the channel. It is assumed that the electrical resistance throughout the channel.

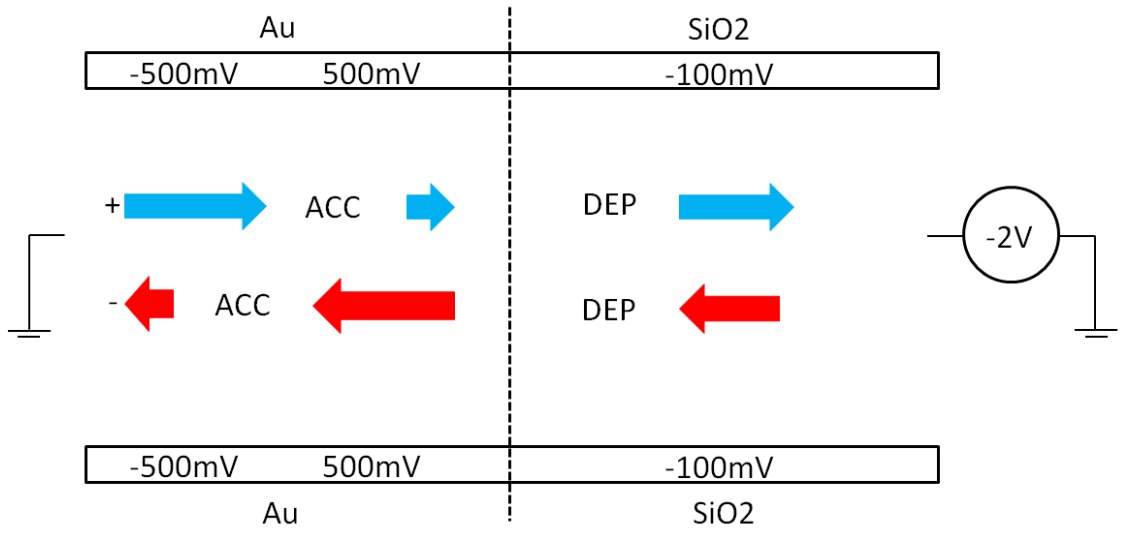

Figure 6: Zeta potential and ionic current immediately after applying a -2V potential difference between the glass side and the gold side of the channel.

When a negative potential of -2V is applied at the glass side of the channel with respect to gold side than the situation of Figure 6 is obtained. Immediately after the application of the electric field, half of the voltage drop occurs at the gold side and the other half at the glass side. At the gold side, this results in a zeta potential varying from -500mV to 500mV. Therefore, positive ions will accumulate at the left hand side and negative ions at the right hand side. Looking at the arrow bars in Figure 6 it becomes clear that there will be an accumulation of charge at the gold electrode and a depletion at the gold-glass junction. Subsequently, the voltage drop will largely occur at the channel junction, which is depleted of ions. Therefore, the conductance of the channel is decreased and the diode is said to operate in depletion.

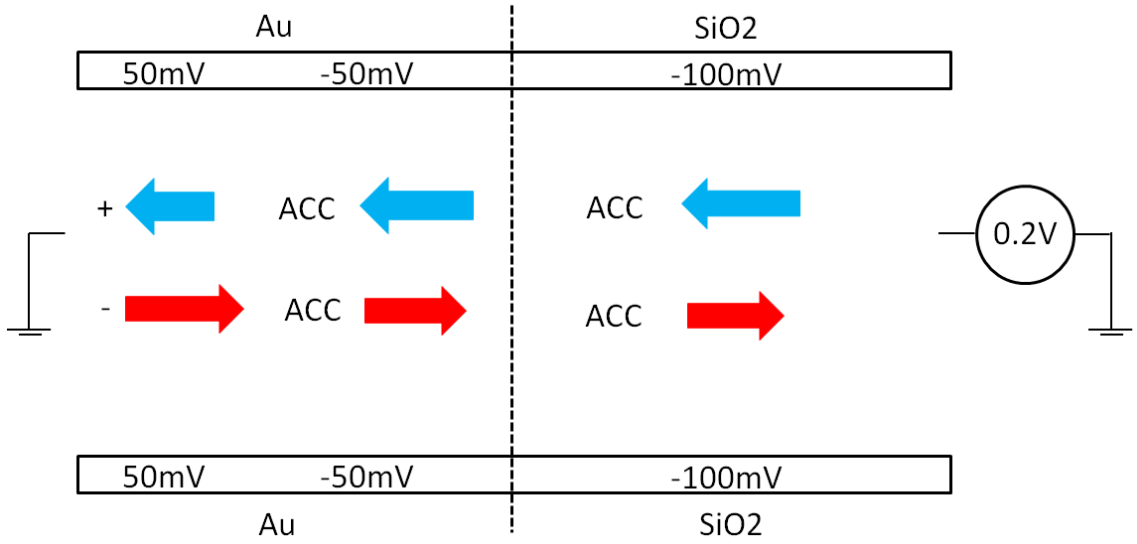

Figure 7: Zeta potential and ionic current immediately after applying a 200mV potential difference between the glass side and the gold side of the channel.

If instead a small positive voltage of -200mV is applied over the channel then the situation of Figure 7 arises. The direction of the polarization of the gold is reversed and the ζ-potential at the

gold side varies from 50mV to -50mV. The arrow bars are drawn again and this time the ions accumulate both at the gold side of the channel as well as at the gold-glass junction. Therefore, the conductance of the channel is increased and the diode is said to operate in accumulation.

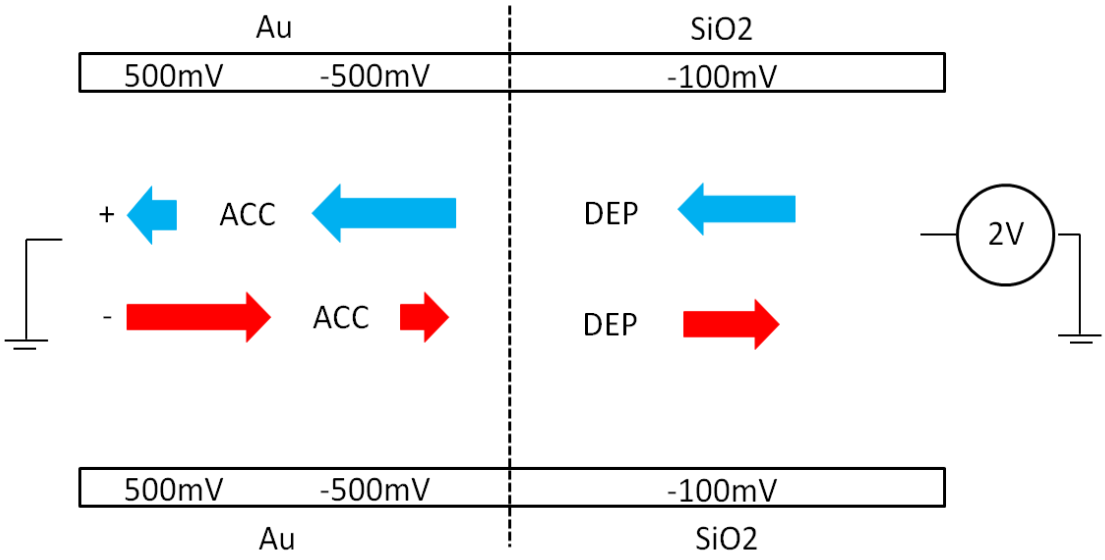

Figure 8: Zeta potential and ionic current immediately after applying a 2V potential difference between the glass side and the gold side of the channel.

Further increasing the potential over the channel to 2V gives the situation of Figure 8. Now, the ζ-potential of the gold at near the channel junction has exceeded the ζ-potential of the glass. That means that ions no longer accumulate at that junction and even deplete again. The diode again operates in depletion. This means that the gold-glass junctions is always reversed biased except for low voltages over the channel where the glass side is at the highest potential. The junction can be biased in accumulation for higher voltages, however, when capacitive control is used to change the ζ-potential of the gold.

2.6 Surface conduction in micro- and nanofluidic channels

Surface effects gain in importance when systems are scaled down to micro or nano levels. This also holds for electrical resistance in small channel. In large channels the electrical conductance is determined similar to that of a wire. The conductance depends on length, cross section area and the specific conductance of the medium

$$S_{ch} = \frac{w \cdot h}{l} \Lambda° c \tag{1.36}$$

With *l*,*b* and *h* the *length*, *width* and *height* of the channel in meters, Λ° the equivalent ionic conductivity in m^2S/mol^{-1} and c_b the concentration in mol/m^3. This type of conductance is called bulk conductance. The specific conductance of a salt solution increases with its concentration. Therefore, the resistance of a channel is expected to increase with decreasing concentrations.

However, there is an additional, concentration independent contribution to the total conductance due to charge transport at the surface of the channels. In large channels, these contribution are much smaller than the bulk conductance and can be neglected. However, for

certain salt concentrations and channel geometries, this surface conduction actually dominates the charge transport.

The resistance of a channel is determined by its surface conduction when $h/\lambda_D \ll 1$ and $c \ll \frac{|\sigma|}{eN_A h}$, that is when the Debye screening length is much larger than the channel height and the ratio of the surface charge density and the height of the channel is large compared to the solute concentration. Now, the conductance of the channel is given by [12]:

$$S_{ch} = |\sigma|\mu w\left(1 + \frac{4\epsilon\epsilon_r k_B T}{e\mu\eta}\right) \tag{1.37}$$

With μ the counter ion mobility. The first term in the brackets of Equation (1.37) represents the contribution of electrophoretic transport of ions and the second term the contribution of electroosmosis.

2.7 Surface coating of gold layers

Gold has two disadvantages as a surface material. It is hydrophobic and molecules are easily adsorbed to the surface. Both problems can be solved by using coating the surface of gold with a thiol. Thiols (R-SH) are known to have a strong affinity for gold. The bond is thougth to originate from the elimination of the hydrogen from the thiol group, while the gold gets oxidized [13].

$$R\text{-}SH + Au_n = R\text{-}S^-Au^+Au_{(n-1)} + ½\ H_2 \tag{1.38}$$

The weak bond between thiolate ($R\text{-}S^-$, where R is any organic group) and gold allows for lateral diffusion of molecules and the creation of a monolayers on the gold surface.

The terminal group of the thiolate can be chosen such that the surface obtains the desired characteristics. An hydroxyl group, for instance, will make the surface hydrophilic. The carbon chain to which the hydroxyl group is connected makes it harder to deprotonate than a hydroxyl groups at the glass-liquid interface.

3. Design of fluidic structures

The design and realization of the fluidic structures with embedded gold surfaces are discussed in this chapter. First, some general features of the fabrication process and experimental setup that influence design choices are briefly considered. Then, the design of the electroosmotic flow pump is presented, followed by a description of the ionic current rectifier. Both structures are created on the same wafer, which imposes constrictions on the design. Additionally, an approach to lower the required gate voltage for surface charge control is introduced. Finally, the fabrication process is discussed in detail.

3.1 General considerations

Some general knowledge of the properties of the fabrication process, the kind of experiments that will be performed and the experimental setup have to be considered as they influence design choices.

A common and straightforward way to create fluidic channels is to etch them in a glass wafer. Subsequently, a second wafer is bonded on top of the first one to seal the channels. The top wafer has holes in it that partly overlap with the channels so that they act as fluidic inlets and the channels can be filled with liquid. The wafers have a thickness of 500µm each. The minimum channel height that can be etched reliably is about 50nm.

It is important to check if any bubbles remain in the channel after they are filled. This inspection requires a microsope. It is therefore useful to use a chipholder that fits on the microscope stage and can also hold the fluidic chip itself. The BIOS group has standardized these chipholders, so that the time that is required to set up an experiment is greatly reduced.

Such a chipholder consists of two pieces as shown in Figure 9. The bottom part is made of aluminum which is anodized to make it harder and to create an electrically isolating layer. The middle of the aluminum plate contains a recessed square, which will hold to top part of the chipholder in place. In that square, a rectangle with the exact dimensions of a chip in recessed even further. Furthermore, there is a hole underneath the chip position which provides an optical window the image the chip from below.

The top part, or cover, is made from polyoxymethylene. It consist of square plate mounted on top a slightly larger square plate, the former of which fits exactly in the recessed area of the bottom part. There are six holes in the cover that provide fluidic access to the underlying chip. These holes can also be used as additional fluidic reservoirs. Furthermore, three steel pins pierce trough the cover so that electrical contacts can be made with the chip. Little springs push these pins against the chip surface to provide a robust connection.

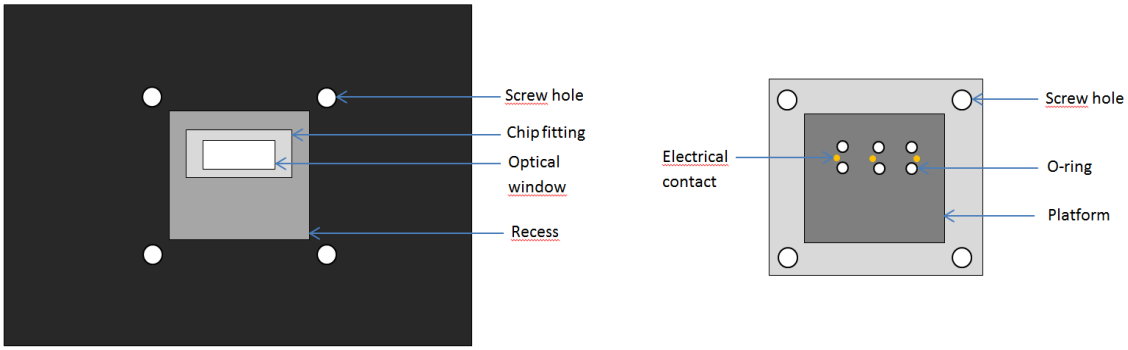

Figure 9: A schematic overview of the chipholder. The left hand side shows a top down view of the bottom part while the right hand side gives a bottom up view of the cover.

This standardized design, however, also requires a standardized chip design. For instance, the inlets of the fluidic chip must aligned with the holes in the cover plate of the cipholder. Therefore, the chip layout of Figure 10 is taken as the starting point for the design.

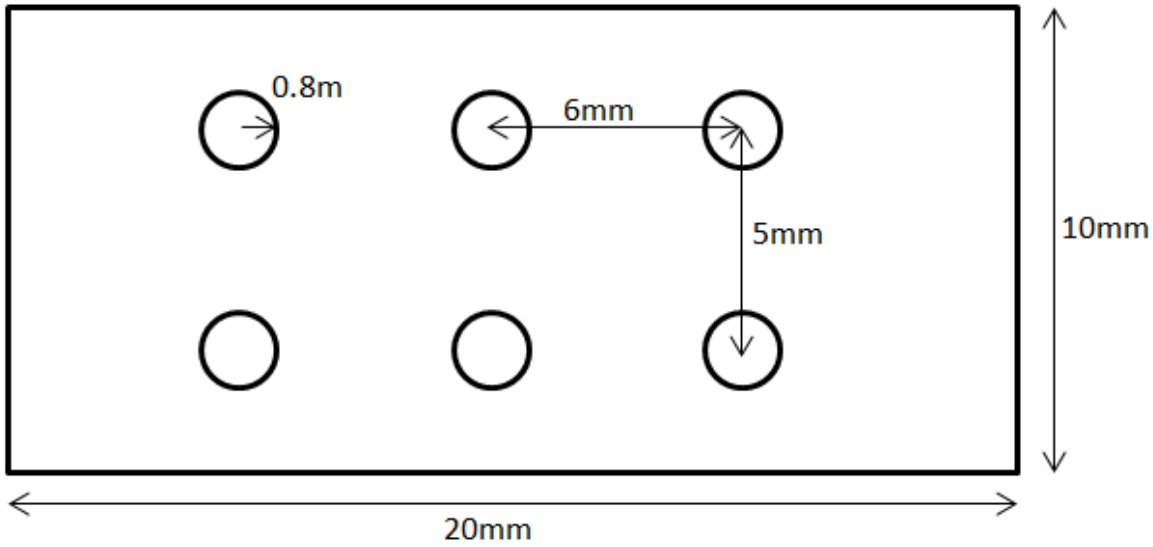

Figure 10: Standard chip layout that fits in a chipholder. The six round inlets are positioned such that they can be reach by the fluidic connections of the chipholder.

3.2 The electroosmotic flow pump

The flow pumps consist of little more than a channel between two inlets over which a potential is applied. Three of such channels can be made by connecting three pairs of inlets in Figure 10. This fixes the length of each channel to 5mm. Moreover, with typical field strength in electroosmotic pumping of 10^4V/m, the potential over the channel can be calculated to be 50V. This potential will create an ionic current through the channel which depends on the electrolyte concentration and the geometry of the channel. The geometry must be chosen such that that current is high enough to be measureable, but low enough so that it does not cause an increase in channel temperature. Moreover, the channel height must be chosen low enough, so that its hydrodynamic resistance is large. The width and height of the channel are chosen respectively 100µm and 20µm. With Equation (1.36), an ion mobility of $7.6 \cdot 10^{-8} m^2/Vs$ and a 50V potential

difference over the channel the current is 320µA for a 1M solution and 32nA for a 100µM solution.

The addition of a gold layer on the surface of the microchannel adds a consideration. That is, if high voltages are applied over the channel, and thus over the gold layer, redox reactions can occur at the boundaries. Electrolysis of water occurs at the edges of the gold layer if there is a potential difference of 1.23V or more over that gold layer. That means that electrolysis certainly occurs when 50V is applied over the channel. To prevent this unwanted effect, the gold layer can be subdivided in electrically isolated strips. Now, instead of a big potential over the entire length of the channel, there is a cascade of potential drops which, individually, are too small to facilitate redox reactions. If these strips have a length of 20µm and a field of 10^4V/m is applied through the channel, then the potential drop over each strip is 0.2V and no electrolysis of water is expected to occur. Glass can be used as the insulating material between the strips, which in this design is equivalent to the absence of gold. The reintroduction of a glass surface inside the channel opposes the goal of making a pH independent pump. However, if the gold strips are much larger than the glass strips in between them, the effect of the glass is minimal. The minimum length of these glass strips are determined by the fabrication process and are 2-4µm.

Another experimental consideration is the visibility of the channel. Ideally, both sides of the microchannel are coated with gold, which make it hard to look inside the channel. One way to characterize the speed of the electroosmotic flow, however, is to optically observe the flow speed of fluorescent beads that are added to the solution. With that method a clear view of the channel is required. Therefore, an optical window is created by removing three consecutive gold strips from the channel. Only strips from the bottom side of the chip have to be removed, as the camera of the microscope that is going to be used images from below.

3.3 The ionic current rectifier

The same connection of inlets as in the electroosmotic flow case can be used to create nanofluidic diodes. Directly connecting two inlets with a nanochannel, however, gives rise to two problems. At 5mm in length, such a long channel combined with the low height of a nanochannel yields a very high electrical resistance and therefore difficulties in measuring the currents. Furthermore, the fabrication process dictates that the inlets are made after the nanochannels are created. Therefore, small particles or other debris that is released during the fabrication of the inlets can clog up the channels. To solve both problems, microchannels are used to interface between inlet and nanochannel. This requires the use of two additional inlets so that there is only room for one ionic current rectifier per chip. A top down view of the positioning of the nanochannel between the microchannels is schematically drawn in Figure 11.

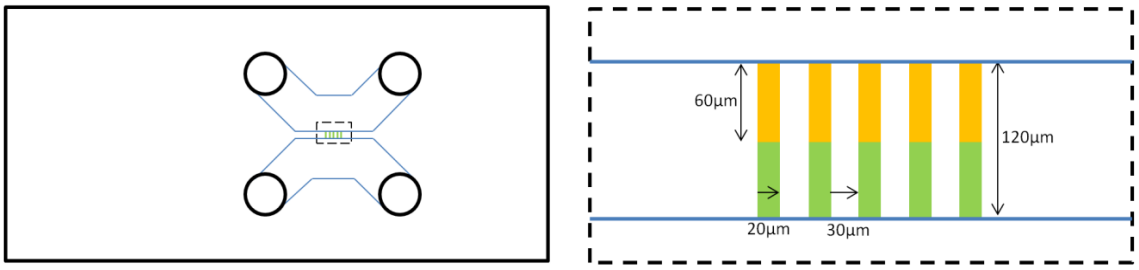

Figure 11: The left images show a top down view of the current rectifier chip. The blue represent the boundaries of the microchannels. The microchannels are connected by five nanochannels. The area in the dashed box is magnified and shown in the figure on the right hand side. The nanochannels are shown in green and the gold surface in orange.

The current rectification effect takes place in the nanochannels. It is not possible, however, to apply a voltage directly over those channels directly. Electrodes are located at the fluidic inlets, which means that part of the voltage drop will be over the microchannels. Therefore, the electrical equivalent circuit will be that of Figure 12. There, the nanochannel is modeled as a voltage dependent resistance. The dimensions of the fluidic channels must be chosen such that the resistance of the nanochannels is much higher than that of the microchannel. In that case the micrchannel resistance can be neglected.

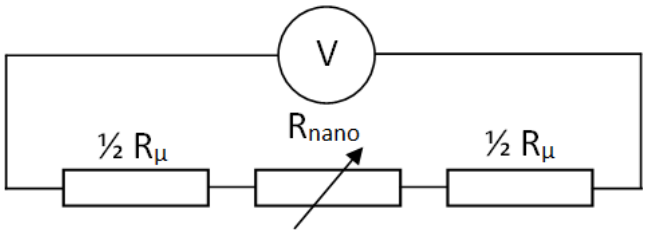

Figure 12: Electrical equivalent system of the micro- and nanochannel series resistance.

First, the geometry of the nanochannel is considered. From Equations (1.26) and (1.29), it follows that the forward current density increases with the an increased fixed charge density while the saturation current decreases. Furthermore, from Equation (1.25) it can be seen that the fixed charge density is inversely proportional to the channel height. Therefore, the height of the channel is chosen as small as achievable in fabrication, which is about 50nm.

Wide channels are preferred as they are harder to clog up with debris or blocked by bubbles. Five such wide channels are constructed next to each other which makes exceedingly unlikely for one bubble to block all channels. The length of the nanochannel must be chosen short enough so that the current trough it is measurable, and long enough so that the resistance of the nanochannels is much larger than the resistance of the microchannels. That current, of course, depends on the applied potential. It is important to consider that one half of the glass channel will be coated with gold to create a junction. That also means that about half of the potential drop is over the gold side. As the potential drop over the gold must be under 1.23V to prevent electrolysis, the total voltage drop over the channel should be well below 2.5V. Now, the current though the channel is still measureable at that potential for a nanochannel length of 120 µm. Equation (1.36) and (1.37) are used to calculate the concentration dependent conductance of

the nanochannel. The results are calculated for a Na_2HPO_4 buffer solution with an $\Lambda°$ of $21.4 \cdot 10^{-3} m^2 S/mol$ [14] shown in Figure 13. The surface charge is of glass of $-60 mC/m^2$ [12] is used for all surfaces, including those of gold. This means that the surface charge conductance of the nanochannel is probably overestimated. The current trough the nanochannel when a 2V potential drop is applied over the channel is still expected to be a couple of nA, which is large enough to measure with standard lab equipment.

Subsequently, the geometry of the microchannel is chosen to maximize its conductivity. The height is 20µm so that it is equal to the height of the microchannel in the flow pump and both channels can be made during the same process step. The length of the channel is minimized by connecting two adjacent inlets, while still reaching the nanochannels and is 17mm. The width is 1.6mm, which is equal to the diameter of the inlets. Using these values it is possible to calculate the conduction of the microchannels at different salt concentrations. Also, the conductance of the micro- nanochannel series combination can be calculated. Both results are shown in Figure 13.

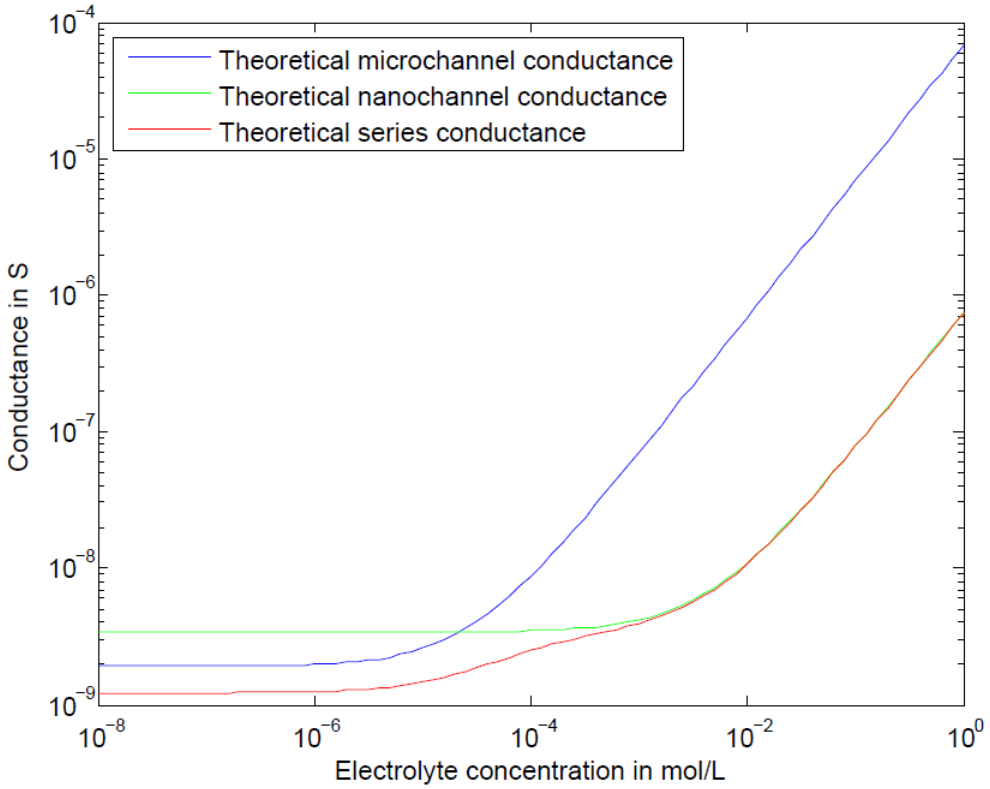

Figure 13: The electrical conductance of the micro- and nanochannels in the current rectifier chip for different electrolyte concentrations according to Equations (1.36) and (1.37). With $\mu=5.3 \cdot 10^{-8} m^2/Vs$, $\epsilon_r=80$, T=300K and $\eta=8.9\ 10^{-4} Pa \cdot s$ [14].

From Figure 13 it follows that the conductance of the nanochannel is more than an order of magnitude smaller than the conductance of the microchannels for bulk concentration of 1mM and higher. Therefore, the electrical resistance of the combined system will be dominated by the nanochannel resistance and the microchannel resistance can be neglected. For bulk concentrations under 1mM, however, the microchannels start to have a significant influence.

3.4 The addition of capacitive surface charge control

It is important obtain an estimate of the gate potential that is required to a significant change on the surface potential. It makes sense to strive for induced surface potentials comparable to those of a glass-liquid interface, which is approximately -100mV at neutral pH. This enables an electroosmotic flow speed which is equal to the flow in a glass channel and, additionally, which directionality can be switched. Moreover, it gives a glass-gold junction to operate as a resistor when their respective surface potentials are equal and to operate as a current rectifier when their surface potentials are opposed in sign.

First, a gate electrode must be created. An easy solution is to position it at the outside of the glass, right on top of the channel. This way, the gate electrode and the floating gold surfaces inside the channel form a parallel plate capacitance, spaced by one wafer thickness. Then the system of Figure 5 is obtained, where the insulator material is the glass wafer. The gate electrode can be painted on the glass or a simple piece of aluminum foil can be used and no extra fabrication steps in the cleanroom are required.

The insulator capacitance is approximated by the model of infinite parallel plates. The capacitance per unit area is than given by Equation (1.30) and depends on the spacing between plates and permittivity of the dielectric between the plates. An insulator thickness of 500µm and a relative permittivity of glass of about 4 results in a capacitance of 70nF/m^2.

The double layer capacitance is approximated similarly, with a plate spacing equal to the Debye screening length. From Equation (1.1) it follows that the Debye length of a 1mM symmetrical electrolyte is approximately 10nm. The relative permittivity of water is about 80, resulting in a double layer capacitance of 70mF/m^2. Substituting these values for the capacitances and the desired 100mV surface potential in Equation (1.31) yields a gate potential of 100kV.

Such high voltages are not only dangerous, but also pose experimental challenges because they can lead to breakdown of air or other materials. Therefore, the required gate voltage should be reduced which means that the insulator capacitance should be increased. There are two possibilities to achieve this, either the plate spacing should be decreased or the plate size should be increased.

The plate separation can be decreased by etching away part of the wafer at the location of the gate. It is assumed that the wafer can be etched back to about 50µm while preserving the structural integrity. However, even after a 10 fold reduction of the plate separation distance, the required gate voltage is still 10kV and the same experimental issues exist. Moreover, the etching requires additional work in the cleanroom. Other designs have been shown with submicron insulator layer thicknesses [2], but these structures are difficult to fabricate and very delicate.

The second option is to increase the area of the insulator capacitance, while keeping the area of the double layer capacitance constant. The trick here, is that the capacitance of a parallel plate capacitor is determined by the smallest plate. Now, if the floating gold surface in the channels is extended beyond those channels, then that would not increase the area of the double layer capacitance. However, if the gate electrode is extended equally, than the insulator capacitance is increased. These extension are referred to as “flaps”.

The flaps for the electroosmotic flow chip are created by extending the gold strips beyond the channel. The length of these flaps are varied between microchannels. This variation makes it possible to create very large flaps for the middle channel if the flaps on the side channels are smaller. Moreover, the variation in size creates the opportunity the characterize the influence of the flaps experimentally. The flaps sizes are chosen such that the insulator capacitance area to double layer capacitance area ratio varies from 1 to 76 with steps of 15. That means that for the channels with the biggest flaps the required gate potential is reduced to 1.3kV. A top view of the resulting chip design is given in Figure 14: .

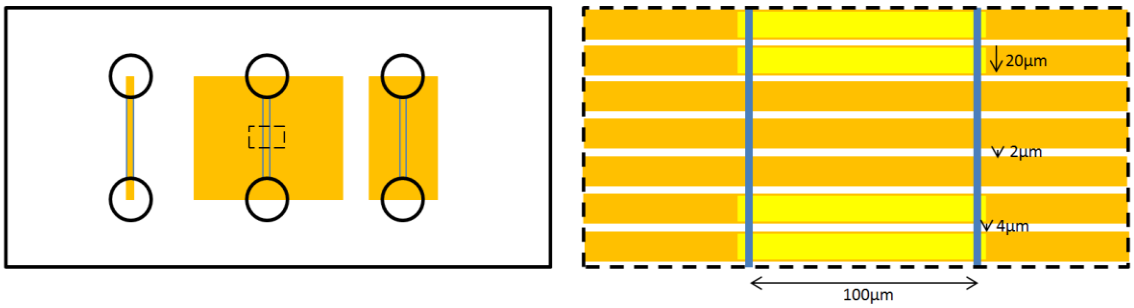

Figure 14: The left image shows a top down view of the an electroosmotic flow chip with three channels each having a different flap size. The blue lines represent the microchannels and the orange rectangle the gold flaps. The area in the dashed box is magnified and shown in the figure on the right hand side. This is a bottom up view. The large flaps are located on the top of the channel. The bottom of the channel is also covered with gold, however, three of the gold strips are removed to provide an optical window to the channel.

The speed of the electroosmotic flow as a function of concentration is also plotted in Figure 15 for a 50V potential difference over the channel and a gate potential of 1kV. The current through the channel as function of electrolyte concentration is also given. Higher salt concentration lead to thinner double layers and therefor lower ζ-potentials, which decreases the speed of the electroosmotic flow. In the Helmholtz model of the electrical double layer, the double layer thickness and hence the ζ-potential scales with the inverse root of the concentration and so does the flow speed. The insulator to double layer capacitance ratio is one, which means that the flow speed can be much higher as it scales linearly with that ratio.

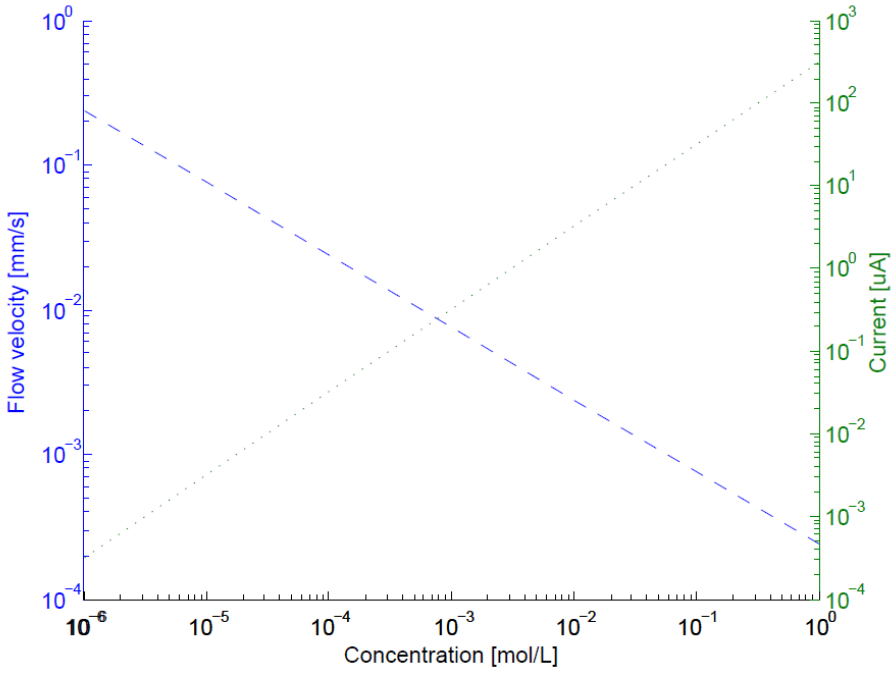

Figure 15: Electroosmotic flow speed and current through the microchannel for a 50V potential difference over the channel and a 1kV gate potential. The insulator to double layer capacitance ratio is 1 and the flow speed is expected to increase linearly with that ratio.

The flap area of double layer area of the current rectifier can be increased even more. Partly, because the total gold-liquid interface in the nanochannels is smaller, but also because there is more room left on a chip to create a large flap. The gold surfaces in the five nanochannels are connected by a gold strip to large gold area. An top view of the resulting chip design can be seen in Figure 16. The insulator capacitance area to double layer capacitance area ratios varied on different chips between 2300, 2600 and 4600. The required potential for the current rectifier with the biggest flaps is now reduced to 20V. Moving the flap away from the microchannel ensures that there is no overlap between the gate electrode and the microchannel, which would increase the double layer capacitance.

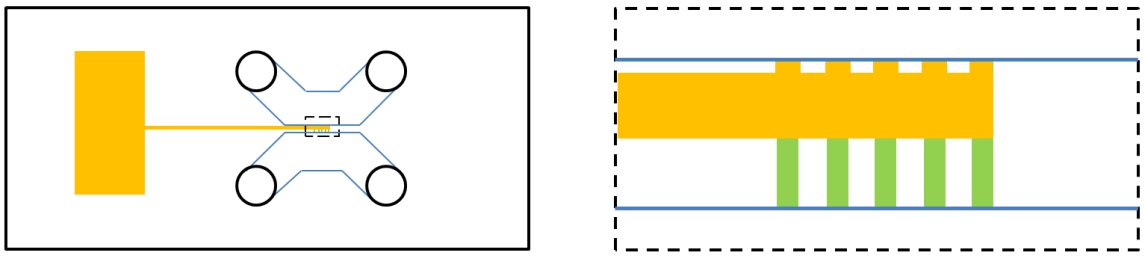

Figure 16: Top down view of an ionic current rectifier chip with a gold flap. The bulk of the flap area is located away from the microchannels. The area in the dashed box is magnified and shown in the figure on the right hand side. A gold strip connects the gold surfaces to the large flap.

3.5 Chip fabrication

The current rectifier and electroosmotic flow chip are made on the same wafer. Or, to be more precise two borofloat wafers that will be bonded together. There are six steps on this process. First, the nanochannel are etched in the wafer that will become the bottom side of the chips.

Subsequently, the microchannels are etched in the same wafer. This etching process is isotropic, which means that the width and length of the channels will be increased by an amount equal to the etching depth. That does not influence the nanochannels much as they are only 50nm deep. The depth of the microchannels, however, is 20µm and their width in the electroosmotic flow pump just 100µm, making a significant addition to the total width.

The third step is the creation of the gold layers in the channels. Both sides of the channel are covered with these surface, however, the additional flaps are only created in the top wafer to prevent bonding issues later on. Gold does not bond to glass very well, therefore, a tantalum layer is placed in between to offer a better connection. The combined thickness of the gold and tantalum layers is about 60nm. This means that the glass has to be recessed before these layers are sputtered on, the nanochannel would otherwise be completely blocked.

The fourth and fifth step are performed on the other wafer that will be used as a cover the close the channel that are etched in the bottom wafer. First, the gold surface are added in the same manner as on the other wafer, that is recessed and with a tantalum adhesion layer. The flaps are also embedded in here. Next, holes are powderblasted trough the wafer to create access to the microchannels. The sixth and final step is the bonding of the wafer.

The resulting structures are drawn in Figure 17 en Figure 18 for the diode and the pump respectively.

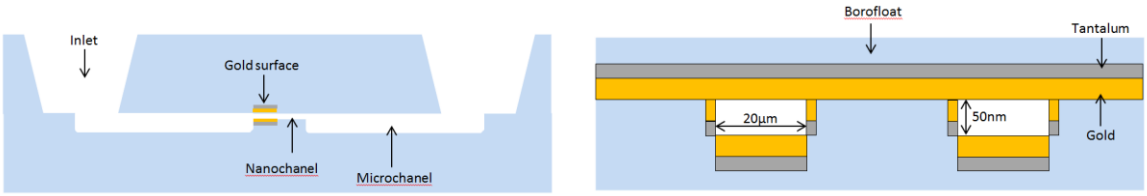

Figure 17: Schematic overview of the a diode chip . The left hand side shows a side view of the current rectifier chip and the right hand side a detail of its cross section.

Figure 18: Schematic overview of the a electroosmotic flow pump chip . The left hand side shows a side view of the pump and the right hand side a detail of its cross section.

4. Characterization and measurement methods

This chapter treats the experimental setups that are created to characterize the fluidic structures. First, frequently used solutions and devices are considered. Next, two different ways to measure electroosmotic flow are presented. Finally, the experiments to characterize the current rectifier are discussed.

4.1 On buffer solution, electrodes and surface coating

A phosphate solution is used for most of the experiments and acts as both a pH buffer and the electrolyte. A 100mM Na_2HPO_4/NaH_2PO_4 solution is created with a pH of 7.4. This solution is subsequently diluted to obtain buffer with a lower molarity. In the rest of this work the phosphate solution is simply called buffer. The conductivity of the buffer is measured with a Mettler Toledo SevenMulti conductivity meter.

The gold surfaces in the channel are coated with 3-mercaptopropanol, which is a thiol with a hydroxyl group at the end. This coating makes the gold hydrophilic and prevents contamination of the gold surface. The thiol is dissolved in ethanol creating a 54mM solution. All chips are placed in a glass beaker with 100mL of the thiol solution and subsequently put in a vacuum chamber for half an hour after which they stay in the solution for another 24 hours. Subsequently, the chips are rinsed and the microchannels flushed with demi-water. Then, everything is placed in a glass beaker with demi-water. Again, the beaker is put in a vacuum chamber for an hour followed by a 24 hour waiting period. Finally, they are dried in an oven at 100°C for four hours to evaporate all liquid from the channels.

Platinum wires are used as electrodes to apply potential differences over the fluidic channels. The electrodes have a diameter of 0.1mm. These electrodes are polarizable, that is, electrical double layers will form at its interface if there is a potential difference between the electrode and the solution. Ideally, non-polarizable electrodes such as Ag-AgCl are used. However, these electrodes require the presence of chloride in the solution. The downside of chloride is that it can dissolve the gold surfaces in the channel.

4.2 Measuring electroosmotic flow

The hydrophilicity of the microchannels is characterized before any flow experiments are carried out. Therefore, a chip containing three microchannels is placed in the chipholder. The chipholder is then placed on a Leica DM IRM microscope. A Hamamatsu ORCA-ER black and white CCD camera is mounted on the microscope and connected to a PC. Demi-water is pipetted into one of the channel inlets and the filling behavior is observed.

An elegant way to measure the electroosmotic flow is vary the conductivity of the solution inside the channel and then monitor the current. This so called Current Measuring Method (CMM), starts with a channel filled with a solution of a known conductivity. If a voltage is applied over the channel, then there will be an electrical current. That current should be constant. Also, if the channel has a non-zero surface potential, the voltage will result in an electroosmotic flow. Now, if the solution entering the channel is replaced by a solution with a higher conductivity, than that high conductivity solution will eventually replace the original solution. Subsequently, the measured current through the channel gradually rises, until all the solution has been replaced with a solution of higher conductivity. At that point the current stabilizes again. Finally, if the

length of the channel is known as well as time is has taken to replace the entire solution than the electroosmotic flow speed can be calculated. The main advantage of this setup is that it only requires one voltage source and a current meter.

During the CCM experiments the chipholder is still placed on top of the microscope. Additionally, a Keithely 2410 SourceMeter is used as both the voltage source and the current meter. A potential difference is applied over a channel using two platinum wires as electrodes. A 5mM buffer solution is inserted in the inlet at the lowest potential and fills the channel. Subsequently, a 10mM buffer solution is inserted at the other inlet completing the electrical path. Now the 10mM solution replaces the 5mM solution due to the electroosmotic flow.

The flow speed can also be determined optically with Particle Tracking Velocimetry. The idea is that fluorescent beads are added to solution. The electroosmotic flow will move these beads through the channel. A fluorescence microscopy setup connected to a computer is used to track to beads and determine their speed. The beads, however, usually have a net charge. This means that the speed of the beads has an electrophoretic component in addition to the electroosmotic flow. Additional experiment to determine the electrophoretic mobility are necessary to isolate the electroosmotic mobility from the speed measurements.

Again the chipholder is placed on the microscope. Moreover, a mercury light source is used for the PIV experiments in combination with a Leica I3 filter cube. That filter cube has a bandpass excitation filter of 450-490nm and a lowpass repression filter with a cut-off wavelength of 515. The beads that are used for these experiments are Estapor fluorescent microspheres F-XC 100. They have a diameter of 1µm, excitation wavelengths of 470 and 490 nm and emission wavelengths of 525 and 560nm and are dissolved in a 1mM phosphate buffer solution. The same Keithely 2410 SourceMeter and platinum electrodes are used to create the potential difference over the channel necessary for electroosmotic flow.

Surface charge control is used in combination with the PIV measurements. First, a gate is painted on the top side of the channel with a silver conductive paste in such a way that it overlaps with the gold flaps within the chip. It is important that the gate does not make direct contact with the solution. Therefore, the area under the reservoirs it the chipholder must be avoided with the silver paste. The silver paste is dried in an oven at 60° for 4 hours. Afterwards, the chip is placed in the chipholder and filled the usual way. Now, a second source meter is used to apply a potential difference between the gate connection on the chipholder and one of the platinum electrodes, which is contact with the solution. The gate potential is varied between -1100V and +1100V and the results are observed with the microsope. An overview of the total setup to perform all types of experiment is given in Figure 19. The equipment that is used depends on the type of experiment that is performed as described earlier.

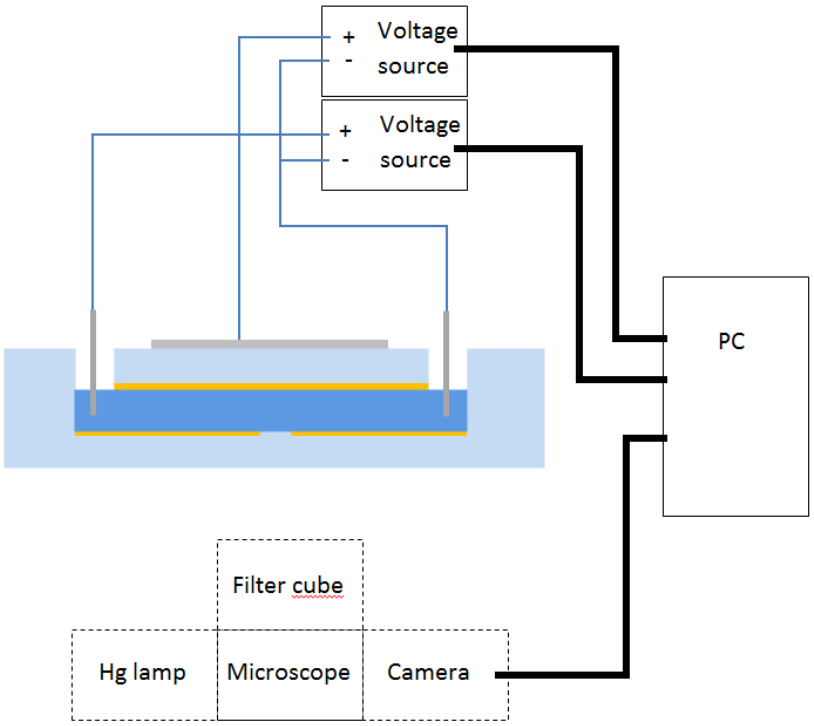

Figure 19: Experimental setup to measure electroosmotic flow. One voltage source is used to create an electric field inside the channel, the other to apply a gate potential. The chip is imaged with a microscope from below, with the possibility to record images with a camera. Moreover, a mercury lamp and a filter cube can be added for fluorescent microscopy.

4.3 Measuring a current rectifying effect

The hydrophilicity of the nanofluidic channels in the diode structure are characterized in the same manner as the microchannels of the EOF pump. That is, the chip is observed through the microscope when the microchannels, and subsequently the nanochannels, are filled.

Next, the conductance of the fluidic circuitry is measured from one microchannel inlet, via the nanochannel to the inlet of the other microchannel. This value is then compared to the conductance if just a single microchannel to check whether the series impedance is dominated by the nanochannels. Therefore, a similar setup as that of Figure 19 is used. The current rectifier is placed in the chipholder and filled with a 1mM buffer solution. Again, a source meter is used to apply a voltage over the channel and measure the current.

The downside of measuring the conductance with a dc voltage is that the current is expected to decrease over time due to the charging of the double layer capacitance. If electrical equivalent circuit of Figure 12 is expanded with the model for the platinum electrodes, the circuit of Figure 20 is obtained. If a voltage is applied over the system of then a current will follow through the resistances. That currents charges the double layer capacitances and creates a voltage drop over the capacitance. That voltage drop, in turn, decreases the potential difference over the channel and therefore the current through the channel. The unknown voltage drop over the capacitances make it difficult to characterize the current rectifier properly.

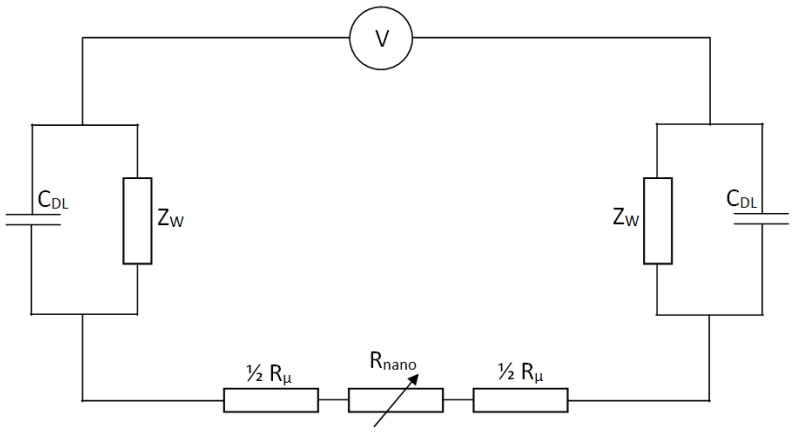

Figure 20: Electrical equivalent circuit of the current rectifier, including a capacitance and Warburg impedance as a model of the electrode-solution interface.

The problem of the double layer capacitance can be circumvented by characterizing the system using Impedance Spectroscopy. In such experiments, ac voltages rather than a dc voltage. The impedance of the capacitance is $1/j\omega C_{DL}$ and decreases with increasing frequency. Eventually, the impedance of the double layer will be much smaller than impedance of the channels and the voltage drop over the double layer negligible. In that case, the measured impedance is that of the channels. An additional bias voltage, however, is still required to create the variable resistance of the nanochannel. The unknown voltage drop over the capacitances due to the bias voltage results again in an undetermined potential drop over the channels. However, if the dc current through the system is known, and the impedance of the nanochannels is known, then the voltage over the channels can be calculated using Ohm's law.

These experiments are carried out with a BioLogic SP-300 potentiostat. The chips are placed in a glass beaker containing a 1mM buffer solution. Then, that container is placed in a vacuum chamber for 15 minutes so that potential bubbles in the nanochannel are dissolved. Afterwards, the chip is dried with tissues and placed in the chipholder. Then, the same 1mM buffer solution is pushed through the microchannels until all reservoirs of the chipholder are full. The electrode are placed in the inlets at opposing sides of the nanochannel. The working electrode is placed at the glass side of the junction. The counter electrode is connected to the reference electrode and placed at the gold side of the channel. Subsequently a potential difference is applied between the working electrode and the reference electrode. An overview of the connections is given in Figure 21.

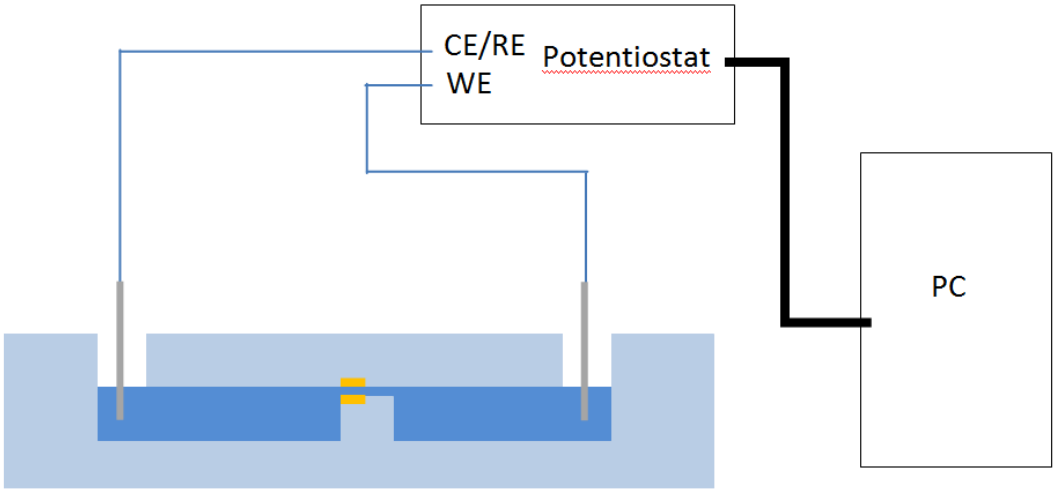

Figure 21: Schematic overview of the experimental setup for Impedance Spectroscopy. The working electrode is in an inlet at the glass side of the nanochannel. The counter electrode is connected to the reference electrode and placed at the other side of the nanochannel.

First, the magnitude of the components of the electrical equivalent system are determined. The electrodes are placed on both ends of a single microchannels. An ac voltage with an amplitude of 100mV is applied over the channel and its frequency is varied from 10^{-2} to 10^{6}Hz. The impedance is subsequently measured at 20 logarithmically spaced frequencies per decade. Each measurement is performed 5 times. The same experiment is carried out for the nanochannel with the exception that this time the frequency is varied from 1 to 10^{6}Hz.

Next, the impedance is measured with a varying dc voltage bias superpositioned on the ac signal. These experiments are only done for the micro- and nanochannel combination. Here, a dc voltage is applied over the channel. Then there is a fixed waiting period t_{wait}. Afterwards, an ac voltage is superpositioned on the bias voltage. An example of such a signal is given in Figure 22.

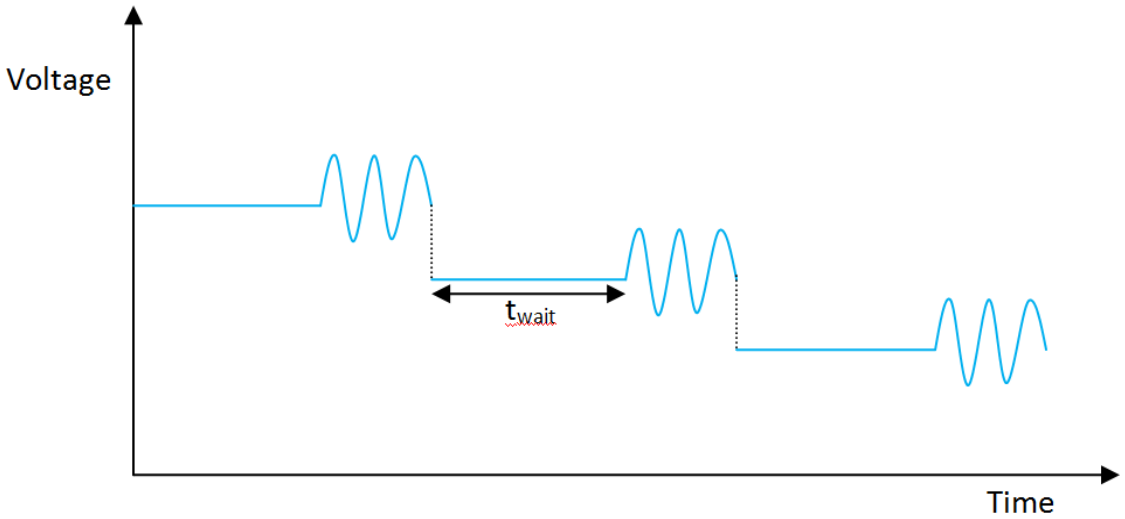

Figure 22: Example of an Impedance Spectroscopy experiment with a bias voltage. A bias voltage is applied for a time equal to t_{wait}. Then, an ac voltage is superpositioned on the dc voltage to measure the frequency dependent impedance. Afterwards, the bias voltage is changed and the process repeats.

The amplitude of the ac voltage is 100mV. The frequency of the sweep varies from 1 $2 \cdot 10^5$Hz. Each measurement is performed 5 times. Finally, after the ac sweep is finished, the bias voltage is changed and the whole sequence repeats.

Five different chips are characterized in this way. The dc bias voltage is swept from -3V to +3V with steps of 0.5V where the potential is defined with respect to the gold side of the channel. Two series of experiments are carried. During the first, the waiting time t_{wait} is one minute. The impedance is measured at 10, logarithmically distributed, frequencies per decade and for each frequency the average of 5 measurements is taken. The second series has a t_{wait} of 20 minutes. Moreover, the impedance is measured at 30, logarithmically distributed, frequencies per decade and for each frequency the average of 10 measurements is taken.

Next, the influence of a gate potential is measured. The required gate voltage are in the order of kilovolts. It is possible that when electrical shorts occur at these high voltages that the machine breaks down. Therefore, it is not attempted to use the potentiostat in combination with a high voltage power supply. Instead, a much cheaper, in house designed lock-in amplifier is used. A lock-in amplifier compares the amplitude and the phase of a signal it generates with the signal it receives after it passes through a system. Such a lock-in amplifier can be used to determine the determine the impedance of the fluidic system as is shown in Figure 23.

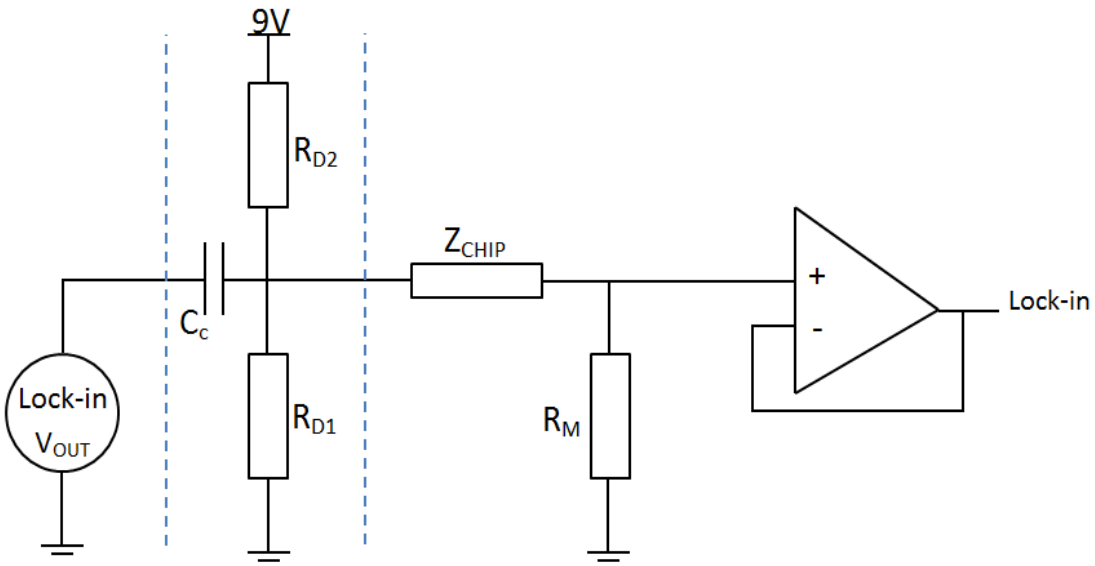

Figure 23: Schematic overview of the experimental setup to measure the nanochannel impedance with a lock-in Amplifier. The part between the dashed lines is optional circuitry to add a dc voltage bias to the signal.

In Figure 23, the signal generator is connected to the fluidic chip which in turn is connected to ground via a 1MΩ measurement resistor R_M. The signal over that resistor is buffered by an opamp and returned to the lock-in amplifier. Now, it is possible to calculate the transfer function of the system and therefore also the impedance of the fluidic circuit.

First, the results of the lock-in amplifier are compared to the results of the potentiostat. Therefore, the chip is again filled with a 1mM buffer solution in the same manner as in the previous experiment. The amplitude of the signal is 0.6V. No dc bias voltage is applied. The

frequency is swept from 10^2 to 10^6Hz. A total of 100 measurements are made which are logarithmically distributed in frequency. Each measurement is repeated only once.

Additionally, these experiments can be done with a bias voltage over the channel and a gate voltage. The lock-in amplifier, however, is not able to superposition a dc voltage on the signal. Therefore, additional components are added to the circuit, which are shown between the dotted lines of Figure 23. It is a simple voltage divider combined with a coupling capacitor. The resistances of the voltage divider are R_{D1}=21kΩ and R_{D2}=66kΩ resulting in a dc voltage of 2.8V. Expressed as the voltage at the glass side of the channel minus the potential at the gold side of the channel it is -2.8V. The voltage over the chip varies if its impedance changes. However, from Figure 13 it follows that $Z_{CHIP} \gg 1M\Omega$ so that this effect can be neglected. A coupling capacitor of 470µF is used, creating a high pass filter in combination with R_{D1} with a cut-off frequency of $1/2\pi RC \approx 1/50$ Hz.

The gate is made with a piece of aluminum foil which taped on to the gate and connected to a power supply fug HCN 7E 12500 positive power supply. The chip is not placed in the chipholder. The resulting setup is shown in Figure 24. The experiments are repeated with a gate voltage of 1, 2 or 3kV. T

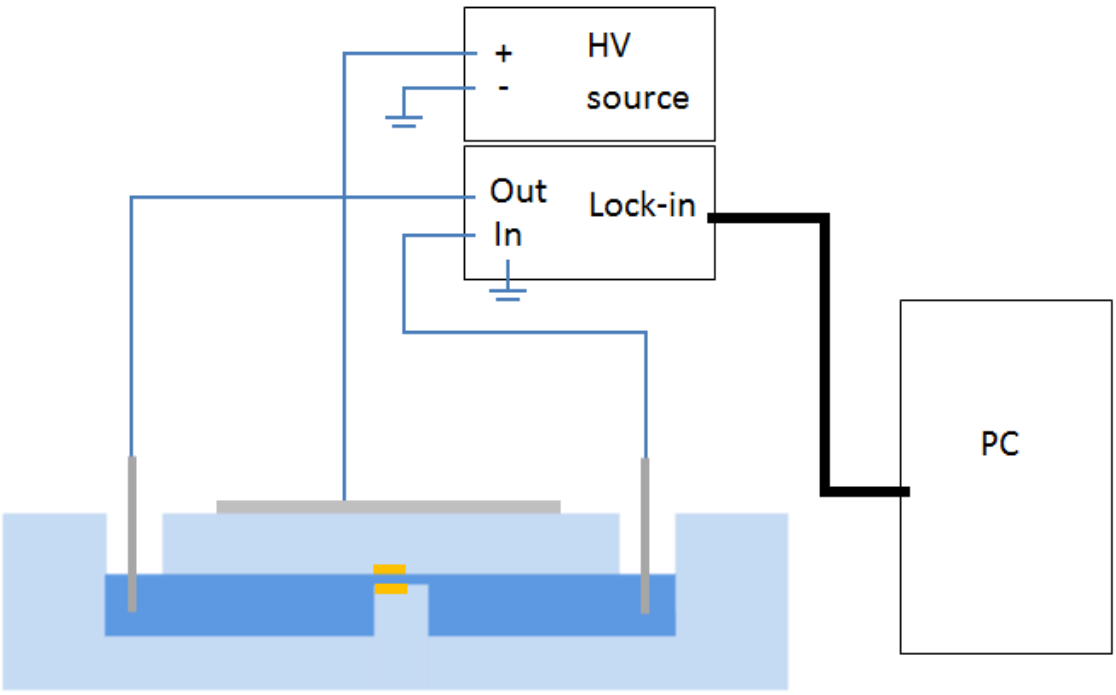

Figure 24: Setup of the lock-in amplifier in combination with a high voltage power supply to apply a gate voltage.

5. Experimental results and discussion

Here, the experimental results are presented and discussed. The chapter is divided in three sections. First, the results of the fabrication process are discussed. Subsequently, the electroosmotic flow experiments are treated. And finally, the characterization of the nanofluidic diode is presented and the its results interpreted.

5.1 Chip fabrication

The chips are optically investigated to check the results of the fabrication process. Figure 25 shows a detail of the gold strips of one of the EOF chips. In the middle, the microchannel can be seen with gold the flaps extending beyond the channel. The dark rectangles are the gold strips at the bottom of the microchannel. Three of them are removed to create an optical window to the channel. The strips are almost black because not the gold but the tantalum adhesion layer is visible from this side.

The gold strips behind the optical window show dark spots. This is probably due to the oxidation of the tantalum adhesion layer, which can occur at the high temperatures that are required for bonding. This, in turn makes the adhesion between the gold and the tantalum weaker, and can cause the gold to detach. The oxygen can most easily reach the surface of the microchannel with explain why the dark spots are not seen in the flaps.

An additional problem is the shorts between electrodes, clearly visible between the strips of the flap. These shorts are formed by what looks like little gold islands. These islands will have a great negative influence on the performance of the EOF chips. The gold strips will be at an equipotential due to these short and therefore greatly diminishing the potential that can be applied over the channel that would not cause electrolysis.

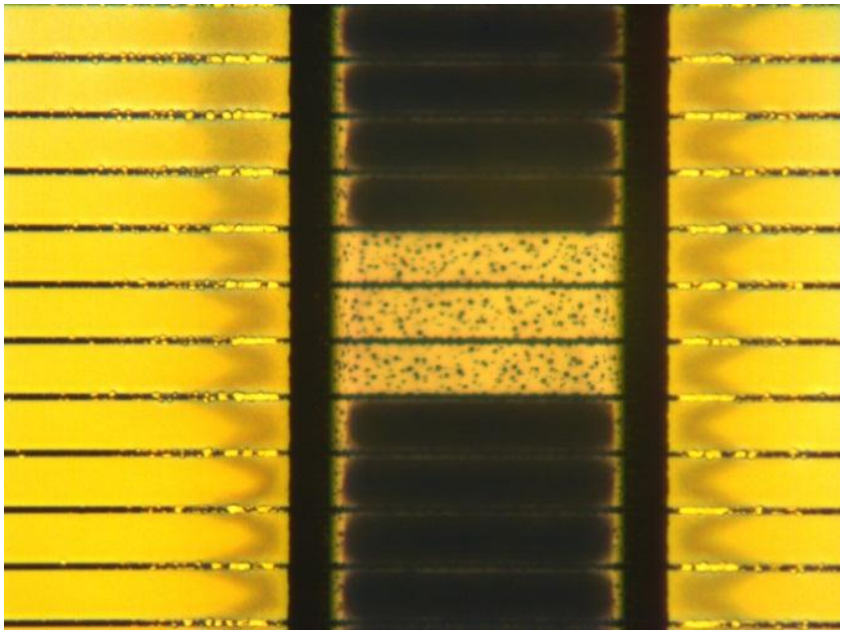

Figure 25: Detail of an EOF chip with, imaged from below. The microchannel can be seen in the middle and is enclosed at both sides by flaps.

The current rectifiers, on the other hand, do not suffer from these issues. As can be seen in Figure 26, the gold in the diodes give good surface coverage without any holes. Moreover, as all

gold in the current rectifier chips is an equipotential, the presence of gold island is of no concern.

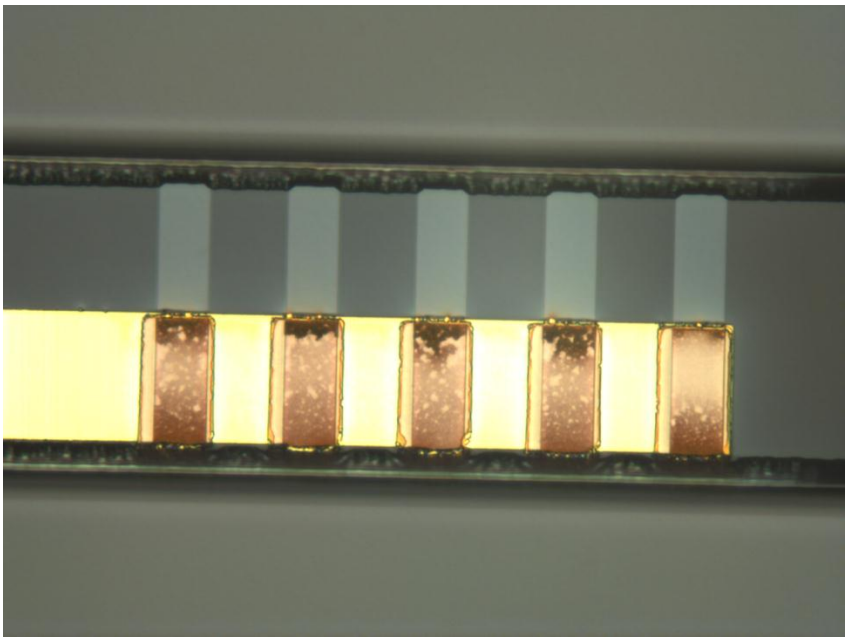

Figure 26: Bottom up view of a current rectifier chip with 50nm gold layers. Microchannels can be seen at the top and the bottom of the image. Five nanochannels connect them and half of the nanochannel has a gold surface. The long strip of gold is at the top of the channel and is connected to a large gold flap, while the five individual strips at the bottom of the channel do not extend more than a couple of micrometer beyond the nanochannels.

5.2 The electoosmotic flow pump

The filling experiments show that the thiol treated microchannels are filled with the aqueous solution by capillary forces. However, the fluids also reach the area adjacent to the channel, where the flaps are positioned. That means that the two wafers haven't bonded perfectly, allowing for an open space to remain between them. It is probable that the bonding is hampered by the gold strips. Although the glass wafer is recessed before the gold strips are sputtered on them, the surface will not be perfectly flat due to deviation in gold thickness along the wafer. This surface roughness and the difficulty of bonding glass to gold may cause the crevices.

The influence of fluid outside the channel on the electroosmotic flow will be minimal as the height of the crevices will be much smaller than the channel height. The leaks can be seen as a parasitic resistance parallel to the channel, not influencing the overall behavior of the system but increasing the power dissipation. The capacitive control of the gold strips, however, is greatly hampered. If the liquid can reach the gold strips outside the channel, than the area of the double layer capacitance will increase just as much as the insulator capacitance and thereby nullifying the flaps influence.

During the current measuring methods experiments it is observed that bubbles were formed in the microchannels for potential differences over the channel between 10V and 20V. These bubbles are thought to be created during the electrolysis of water. The subdivision of the gold layer in strips is supposed to prevent electrolysis for voltages up to 50V. The electrical short between strips, however, have hampered the maximum applicable voltage. Therefore, the voltage is set to 5V for the rest of the experiments in these channels.

The results of the current measuring method for the channels of two different chips are given in Figure 27. Experiments are done with a 5 and 10mM phosphate solution at a potential difference of 5V over the channels. The first subfigure shows the behavior of one of the channels. First, the channel is filled with the low concentration solution, but there is no current as only one reservoir is filled. When the second reservoir is filled with the 10mM solution, an electrical path is created between the two electrodes and the current is determined by the conductance of the 5mM solution and is about 150nA. Then, the current increases as the low conductivity solution is replaced by the high conductivity solution. Then, once the high conductivity solution has completely replaced the original solution, the current stabilizes again at 250nA. The current hasn't doubled as would be expected. This can be due to surface conduction outside the channel.

Some channels behave similarly, as can be seen in Figure 27, although with different EOF speeds. Moreover, some channels don't show a change in current at all. These differences can be explained if there is a pressure driven flow in addition to the electroosmotic flow that increases, decreases or reverses the flow. This assumption can be tested by the particle tracking velocimetry experiments.

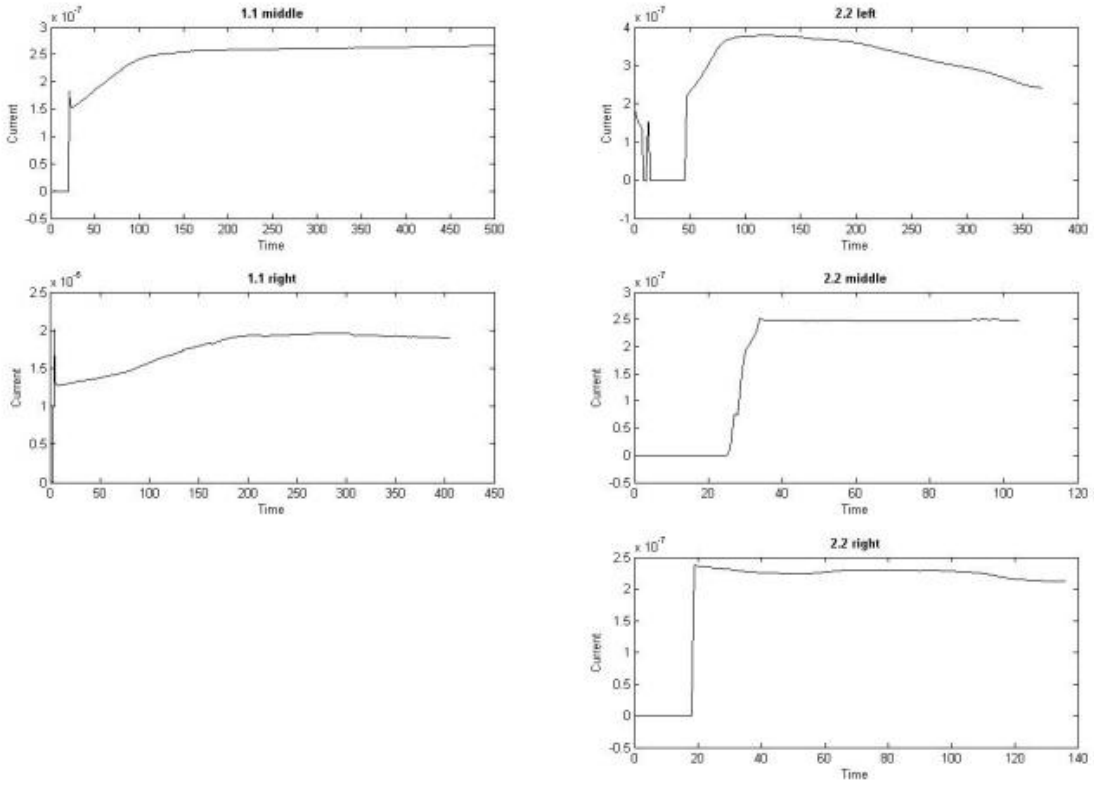

Figure 27: Results of five CCM experiments in five different channels. A 5V potential difference is applied over a channel. A 5mM buffer solution is replaced by a 10mM solution.

A typical image of a particle tracking velocimetry experiment is shown in Figure 28. The 1µm beads are clearly visible, although the focal depth of the microscopy setup is not large enough to image every bead sharply. The beads are confined by the channel. The dark horizontal bars in

the image are the gold strips embedded in the channel. It can be clearly seen that three of such strips are left out of the design to have a clear imaging space.

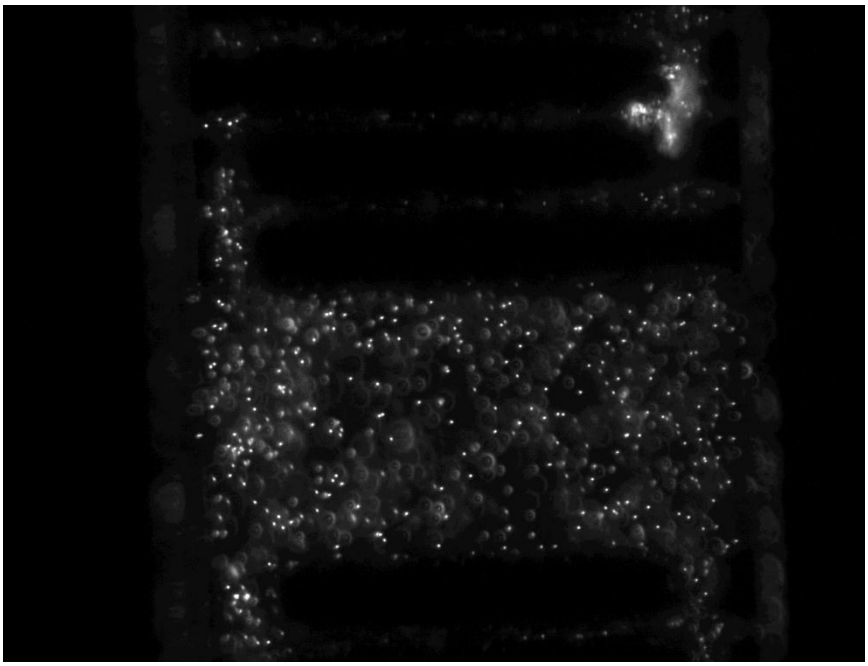

Figure 28: Fluorescent microscopy image of a microchannel filled with 1µm fluorescent beads. An optical window is created by the absence of three gold strips.

The movements of the beads clearly indicate pressure driven flow as even in the absence of any electric field the particles still move through the channel. The pressure driven flow is caused by either a Pascal pressure or a difference in the height level of the solution at both sides of the microchannel. It is attempted to remove the Pascal pressure by forcefully inserting pipette tips in both sides of the reservoir, which have similar surfaces. Subsequently, by carefully controlling the height of the liquid column, the net total pressure driven flow can be eliminated. The resulting setup is very, however, is very delicate and instable. The pipette tips, for instance, are easily displaced. Moreover, the insertion of the platinum electrodes influences the surface tension and creates therefore a Pascal pressure.

However, two observations have been made during experiments. First, the application of 5V potential difference over the channel resulted in a movement of the beads towards the lower potential. As the beads are negatively charged, they move in the opposite direction of their electrophoretic flow. Second, the speed of the beads and therefor the electroosmotic flow is not affected by the application of a gate potential varying from -1.1kV to +1.1kV with respect to the liquid. The absence of this effect is not surprising considering the low gate voltage, the relatively small area of the insulator capacitance and the possibly increased area of the double layer capacitance due to leaks near the flaps.

Due to the limited achievable field strength in the microchannels, the difficulties in removing the pressure driven flow and the ineffective gate potential caused by leaks in the systems, the electroosmotic flow pump is not further investigated and the rest of this work will focus on the ionic current rectifier.

5.3 Nanofluidic structures

The results and discussion of the experiments with the current rectifier is split in three parts. First, the results of the experiment are presented and interpreted with the theory of nanofluidic current rectification. In the second part, an alternate explanation for the results is discussed, which focuses on microchannel phenomena. Finally, the results of the application of a gate potential are discussed.

5.3.1 The nanofluidic current rectifying effect

The filling experiments show that the current rectifier face the same bonding issue as the EOF pump. Therefore, there are leaks between the two microchannel, bypassing the nanochannels. Considering the right hand side schematic of Figure 16, it can be seen that the fluid leaks that are thus created can be split in two contributions. Half of the leakage path between microchannels does not involve the gold strip. Therefore, it can be modeled as a parasitic resistance. Contrary, the other leakage pass crosses both a glass and a gold section. It will therefore have a current rectifying effect, just as the nanochannels. Overall, the current rectifying effect should still be observable, albeit maybe less prominent due to the resistive connection between the microchannels.

Additionally, the filling of the nanochannels is hard to detect optically, as it is impossible to see through the gold side of the channel. Nonetheless, the differences between filling direction implicate poor wettability of the gold. When the fluid arrives from the microchannel connected to the glass side of the nanochannel then the nanochannel is filled immediately. What happens at the gold side of the channel cannot be observed. Accordingly, when the solution arrives enters via the gold side of the nanochannel it is still impossible to observe if that side is filled. However, it is observed that the glass side of the channel is not filled. Therefore, it is assumed that the gold side of the channel cannot be filled by means of capillary forces, despite the use of the thiols. This can either mean that the thiol treatment did not work or that there is a bare surface of the tantalum adhesion layer near the entrance of the channel that is non-wettable.

The current rectifier is expected to suffer from an increased double layer capacitance due to leaks, just as the EOF chip. However, the effect is expected to be much smaller. For instance, the bulk of the flap area is located a large distance from the microchannel. This distance increases the hydrodynamic resistance that the capillary forces have to overcome to reach it. Additionally, in contrast to the EOF chip where the flap is divided in strips, the flap of the current rectifier is a singular piece. This means that the poorly hydrophilic or even hydrophobic gold is hard to reach for the liquid. Moreover the relative flap size of the current rectifier is much larger than the relative flap size of the EOF pump. Therefore, the influence of the increased double layer capacitance is expected to have limited influence over the surface charge control.

The conductance of the microchannel and micro- and nanochannel combination are measured by applying a 1V potential difference over the channels and measuring the currents. The equivalent ionic conductivity $\Lambda°$ is measured for a 100mM buffer to be $18.7 \cdot 10^{-3} m^2 S/mol^{-1}$. Subsequently, the conductance of the channel is measured for buffer solution of 10µM, 1mM, 10mM, 100mM. Additionally, experiments are carried out with demi-water, which is a poorly conducting medium. Demi-water has a molarity of 100nM due its autodisassociation and is used to obtain an estimate of the conductance at very low concentrations. As expected, the current

trough the channels decreases over time. This is attributed to the charging of the double layer capacitance and the subsequent voltage drop over that layer. The highest currents are measured at the moment the voltage supply is turned on. At that point, the double layer capacitance is not yet charged and the resulting voltage drop is minimal. Therefore, the total voltage will fall over the channel and its conductance can be calculated from the resulting current measurement. This is a not a very accurate method to determine the conductance of the channels as the current is not stable and the potential over the double layer unknown. Better measurement methods are required. Nonetheless, it is useful to get a rough idea of the conductance. The results of these experiments are shown in Figure 29 together with the theoretical results. The measurements seem to follow the same trend as the theoretical results.

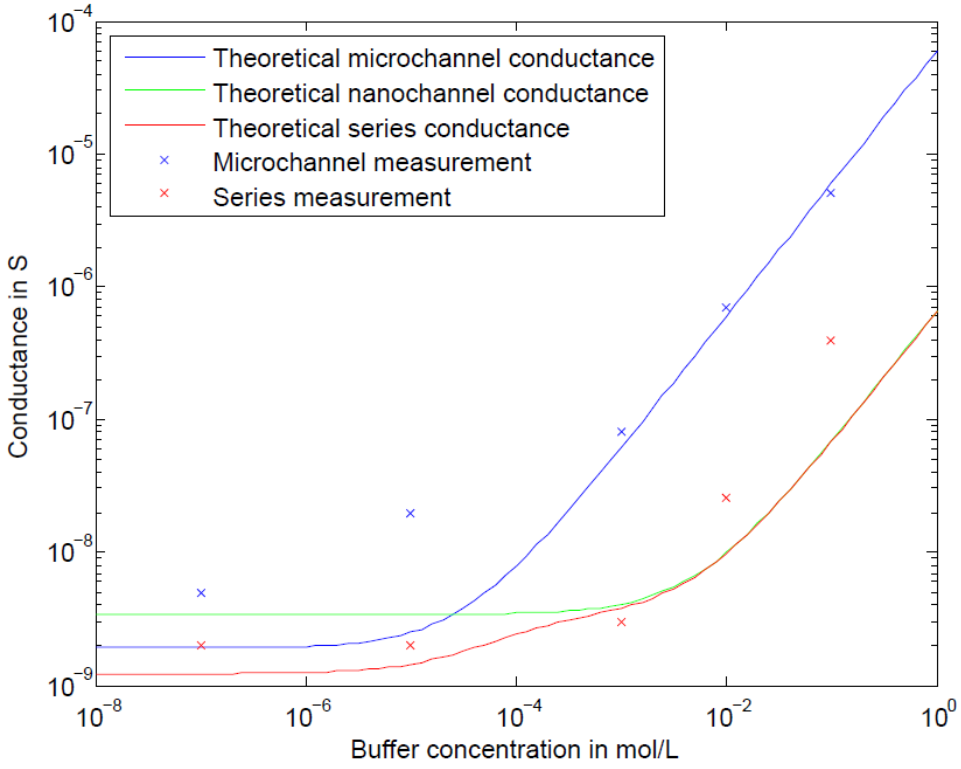

Figure 29: Theoretical and measured conductance of the channels of the current rectifier.

Next, the results of the impedance spectroscopy experiments with the potentiostat are discussed . First, a Bode plot of a 1mM buffer solution in one of the microchannels is made. The result is shown in Figure 30. For low frequencies, between 0.01Hz and 0.1Hz, the impedance has negative slope and a negative phase. At these frequencies, the impedance is expected to be combination of the double layer capacitance of the electrode and the microchannel resistance. This claim is supported by an estimation of the charging time. The electrode has a diameter of 0.1mm and is inserted around 5mm deep into the solution. Combined with the previously calculated double layer capacitance of 70mF/m^2 for a 1mM solution results in a 110nF capacitance. The channel resistance is about 7MΩ. Therefore, the frequency at which the double layer impedance equals the channel impedance is $f=1/2\pi RC=0.2$Hz, which corresponds well with the measured behavior. For frequencies between 0.1Hz and 10kHz, the impedance is constant and the phase is roughly zero. A clear resistive plateau emerges with a magnitude of about

6.8MΩ. Now, the double layer impedance is much smaller than that of the channel. The measured channel resistance, however, is less than half the theoretically predicted 16.3MΩ. This decreased conductance might be due to contaminations from previous experiments as the measured impedance corresponds to an buffer concentration of 2mM. For frequencies above 10kHz, the impedance decreases again and the phase approaches -90°. This is attributed to a parasitic capacitance parallel to the channel.

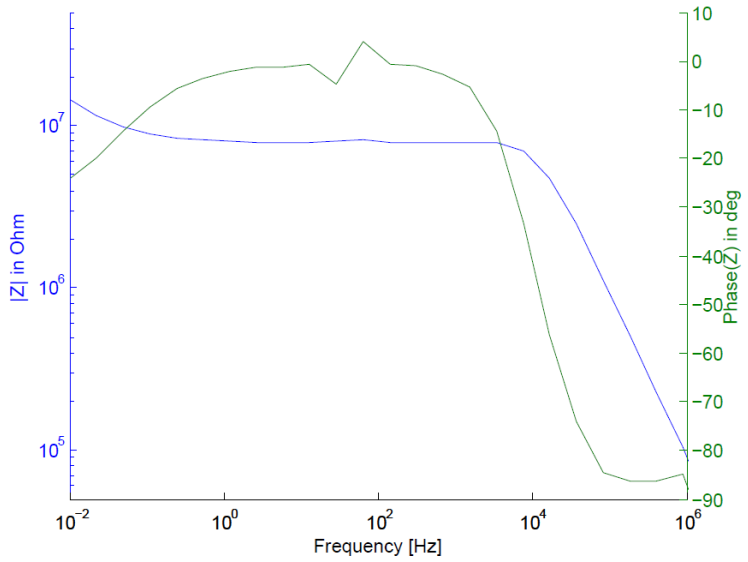

Figure 30: Bode plot of one of the microchannels of the current rectifier filled with a1mM buffer solution.

Subsequently, the experiment is repeated for a nanochannel. The result of one such an experiment is given in Figure 33, where the frequency is swept from 1Hz to 200kHz. For frequencies between 1 and 10kHz there is a plateau again. However, the plateau is slightly tilted for between 1Hz and 100Hz. Moreover, at those frequencies there is a bump in the phase, indicating the presence of a capacitive impedance. For frequencies between the 100Hz and 10kHz the phase goes to zero again and the impedance is a factor of 2 smaller than at the lowest frequencies. The impedance varies between 10MΩ and 20MΩ. For frequencies above 10kHz the impedance decreases and the parasitic capacitance starts to determine the impedance again.

The impedance observed between 1Hz and 10kHz is an order of magnitude smaller can the calculated 260MΩ and the similar value of the experimental results with a dc measurement. This difference might be due to leaks between the microchannels. Even if there is a very small gap, a large increase in conductance is expected due to surface conduction. The microchannels are closely spaced over a length of 2mm, as can be seen in Figure 11, which is more than an order of magnitude longer than the combined nanochannel width. From Figure 29, it can be seen that for a 1mM buffer solution, the bulk conduction and surface conduction in the nanochannels are in the same order of magnitude. Consequently, if the surface conductions is increased 10 fold, then the total channel conductance will also increase 10 fold. A current rectification effect may still occur, as half of the leakage path has an gold strip in between and the total channel resistance is still slightly higher than the microchannel resistance.

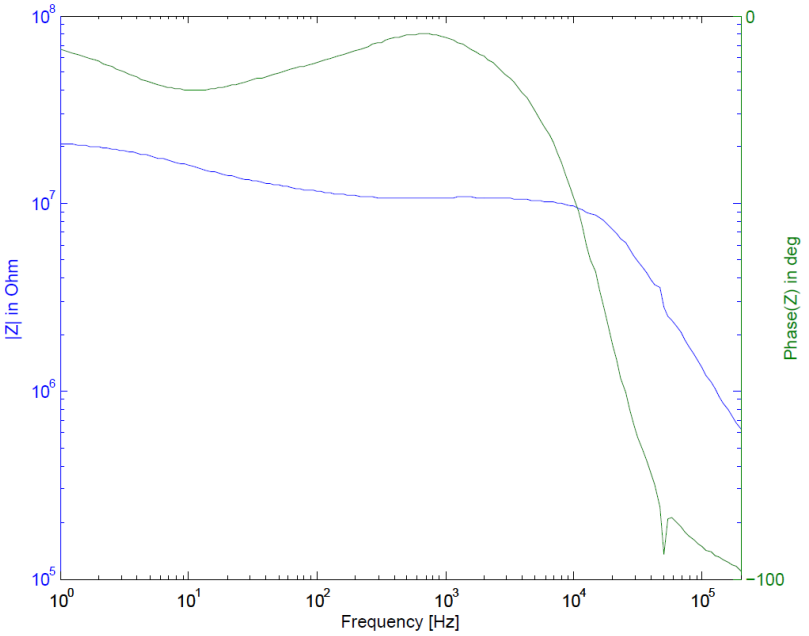

Figure 31: Bode plot of the micro- nanochannel combination of the current rectifier filled with a 1mM buffer solution.

The bump in the phase and the change in impedance by a factor of two is seen in multiple experiments. This phenomenon can be explained by charging effects of the gold surface in the nanochannels. When the potential over the nanochannel changes, then so does the ζ-potential of the gold surface according to Equation (1.35). This process is very fast because gold is a very good electrical conductor. As a result of the changed ζ-potential, the double layer capacitance will be charged at one end of the gold surface and discharged at the other end. This effect can be modeled as a capacitance parallel to the resistance of the gold side of the nanochannel. This capacitance and the previously found parasitic capacitance are added to the electrical equivalent system to obtain the circuit of Figure 32: Electrical equivalent circuit of the current rectifier, including a capacitance parallel to the gold part of the nanochannel.

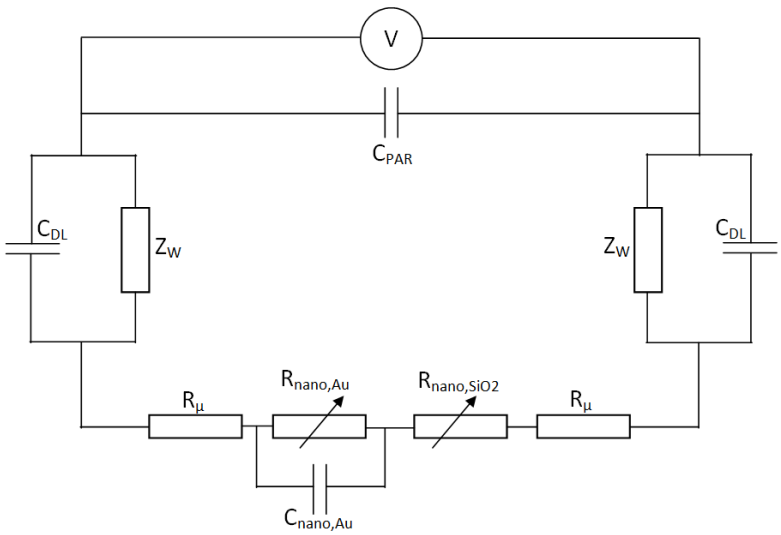

Figure 32: Electrical equivalent circuit of the current rectifier, including a capacitance parallel to the gold part of the nanochannel.

The double layer capacitance of the gold surface in the nanochannels can be calculated so that the frequency at which its impedance equals that of the channel resistance can be determined. The combined width of the nanochannels is 100µm and the length of the gold surface is 60µm. A double layer capacitance per unit area of 70mF/m^2 for a 1mM solution yields a capacitance of 420pF/m^2. If the total resistance of the channels is determined by the nanochannels and if the gold side of the channel accounts for half of the nanochannel resistance, then that resistance is 10MΩ. The characteristic frequency is f=1/2πRC=38Hz. This corresponds quite well to the Bode plot of Figure 31. For frequencies under 1Hz, the impedance of the capacitance much higher than the resistance of both the gold and glass sides of the channel. The impedance is determined by the series resistance of the channel halves and the phase is zero. Around 10Hz, the impedance of the capacitance is in the same order of magnitude as the resistance of the gold half of the channel. The series impedance decreases and the phase becomes slightly negative. For frequencies above 100Hz, the impedance of the of the capacitance is much smaller than that of the gold half of the channel. The series impedance is now that of the glass side of the channel and the phase goes to zero again.

Next, a dc bias voltage is added to the impedance measurement. The bias voltage is defined from the glass side to the gold side of the nanochannel is swept between -3V en 3V with a 0.5V step size. The waiting time, t_{wait}, between measurements is 20 minutes, which is much larger than the double layer charging constant. The results are given in Figure 33.

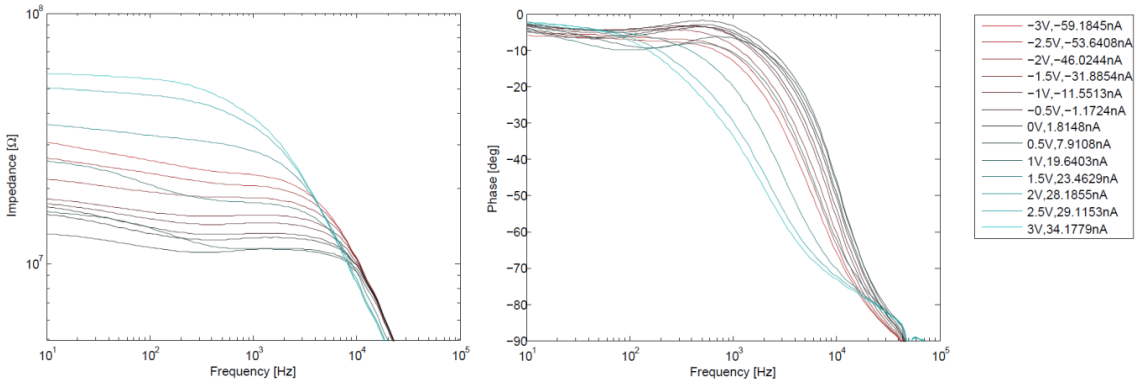

Figure 33: Bode plot of the nanochannels for different dc bias voltages. The left figure show the impedance plot and the right figure the phase plot. A 1mM buffer solution is used. The legend also shows the dc currents at a given bias voltage.

At a glass to gold voltage difference of -3V the diode is expected to deplete of ions and have a high impedance. Indeed, Figure 33 shows that the impedance of the nanochannel decreases with an increasing bias voltage. The nanochannel is expected to accumulate ions at positive voltages, decreasing the impedance even further. However, there is a minimum at 0.5V after which the impedance increase and even exceeds the values found at -3V.

This phenomenon is ascribed to the polarization of the floating gold in the nanochannel. According to Equation the ζ-potential of the gold depends on the potential applied over it . If the ζ-potential of the gold exceeds the ζ-potential in at the gold-glass interface then the diode direction switches. This causes the nanochannel to deplete of ions again as shown in Figure 8.

This explanation is further supported by the results of Figure 34a. Here, the impedance is measured with a dc voltage sweep, resulting in similar results as that of Figure 33. During these

experiments, however, t_{wait} is 1 minute. Subsequently, the impedance at a fixed frequency, in this case 317Hz, is plotted against the voltage bias. The results are shown for the same experiment in five different chips. Four of the five experiments show a similar v-shape and a minimum in impedance slightly above zero. The fifth experiment does not show a current rectification effect at all and its impedance is rather high. Similar plots can be made at frequencies between 1Hz and 1kHz.

Although the applied bias voltage over the two electrodes is known, the exact voltage over the nanochannel is not, because of the uncertainty in the voltage drop over de double layer. This voltage, however, can be calculated from the experimental data. The impedance of the nanochannel is found from the resistive plateau in the Bode pot. Moreover, due to current continuity, the current due to the bias voltage measured at the electrodes also flows though the nanochannel. Multiplying both gives the potential drop over the resistive part of the fluidic circuit. This potential drop is called the effective potential. In Figure 34b the impedance at 317Hz is plotted against this effective voltage for the same five chips. The effective voltage is about 1-1.5V less than the applied voltage, which is also the amount of voltage drop that is expected at the electrodes.

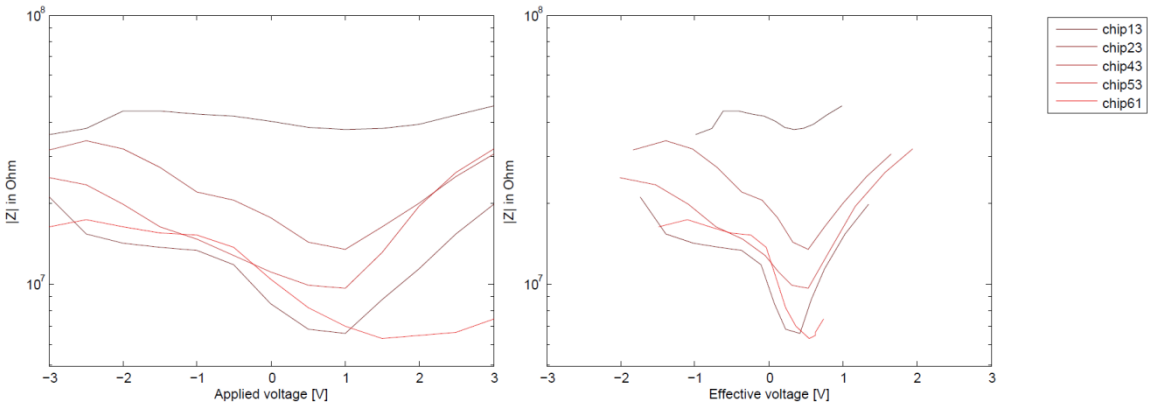

Figure 34: The voltage dependent impedance at 317Hz for five different chips. At the left side, the impedance is plotted against the voltage that is applied at the electrodes. The right side shows the impedance versus the voltage that is calculated to be over the resistive part of the fluidic circuit. Experiments are done with a 1mM buffer solution.

The minimum impedance is found to be around 200-300mV, which is also where the minimum is expected from Figure 7 to be. Subsequently, the same experiments in the same chips are carried out again only with a longer waiting time of 20 minutes. The results are given in Figure 35, where for each chip the results of the experiment with a 1 minute and a 20 minute waiting time are displayed.

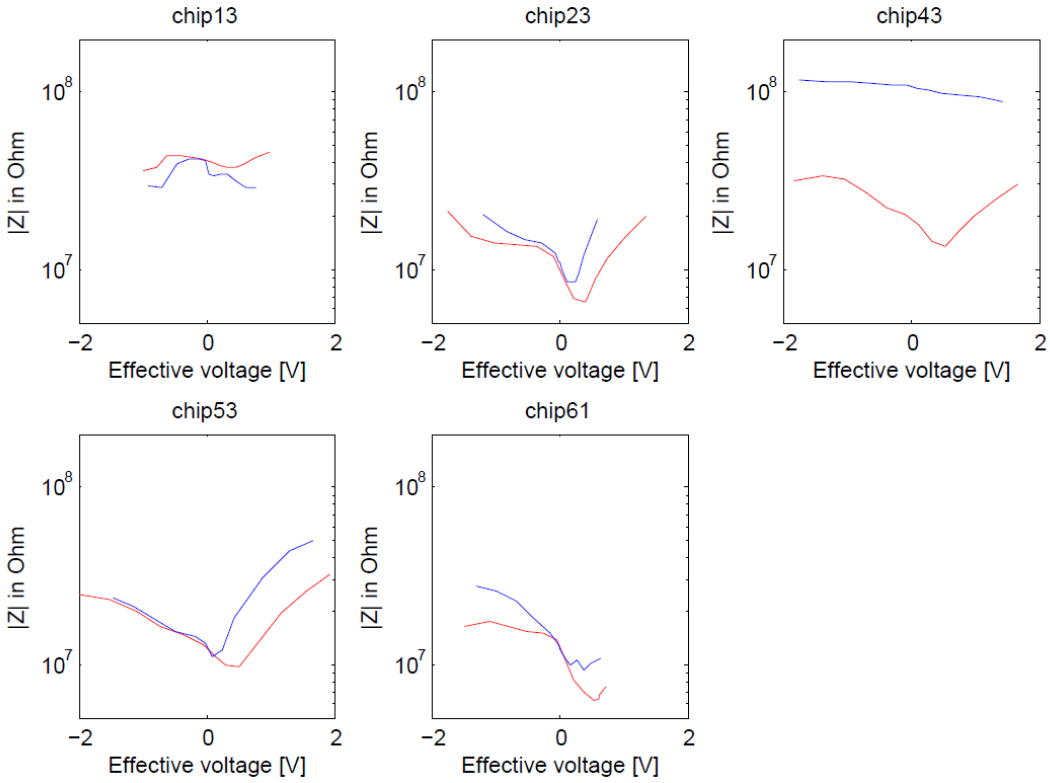

Figure 35: Plots of the impedance versus the effective voltage at 317 Hz for five different chips. The blue lines represent experiments with a t_{wait} of 20 minutes and the red lines experiments with a t_{wait} of 1 minute. Experiments are done with a 1mM buffer solution.

The results of chips 23,52 and 61 all show the same, v-shaped, impedance characteristics. Moreover, the magnitude of the impedances is similar for different chips, with a minimum of around 10MΩ and an impedance of about 20MΩ at higher effective voltages. Chip 43 shows that same behavior for the experiment with a t_{wait} of 1 minutes, but the 20 minute experiment deviates significantly. The impedance is much higher than expected and independent of the voltage. It is possible that a bubble obstructed the channels in this experiment. Chip 13 shows similar results for both experiments, however, no rectifying behavior is observed. Again, this might be caused by bubbles or even structural defects such as blocked nanochannels.

The three chips that do show the v-shaped impedance characteristic, chip 23, 53 and 61, are examined further. It seems that the red graph is shifted to the right with respect to the blue one. Or, considering that the dc voltage bias starts at -3V and then increases, that the red graph lags behind the blue graph. This is unexpected, as any charging effect of the electrical double layer at the electrode interface is accounted for by using an effective voltage.

From the discussion above, it follows that an additional effect plays a role. Therefore, the dc currents and bias voltages that are measured during the impedance spectroscopy are considered. They are shown in Figure 36 for chips 23,53 and 61. The experiments with a 1 minute waiting time are shown on the left and those with a 20 minute waiting time on the right. It can be seen that the current is almost constant during the measurements with a 20 minute

waiting period, but not during the other set of experiments.

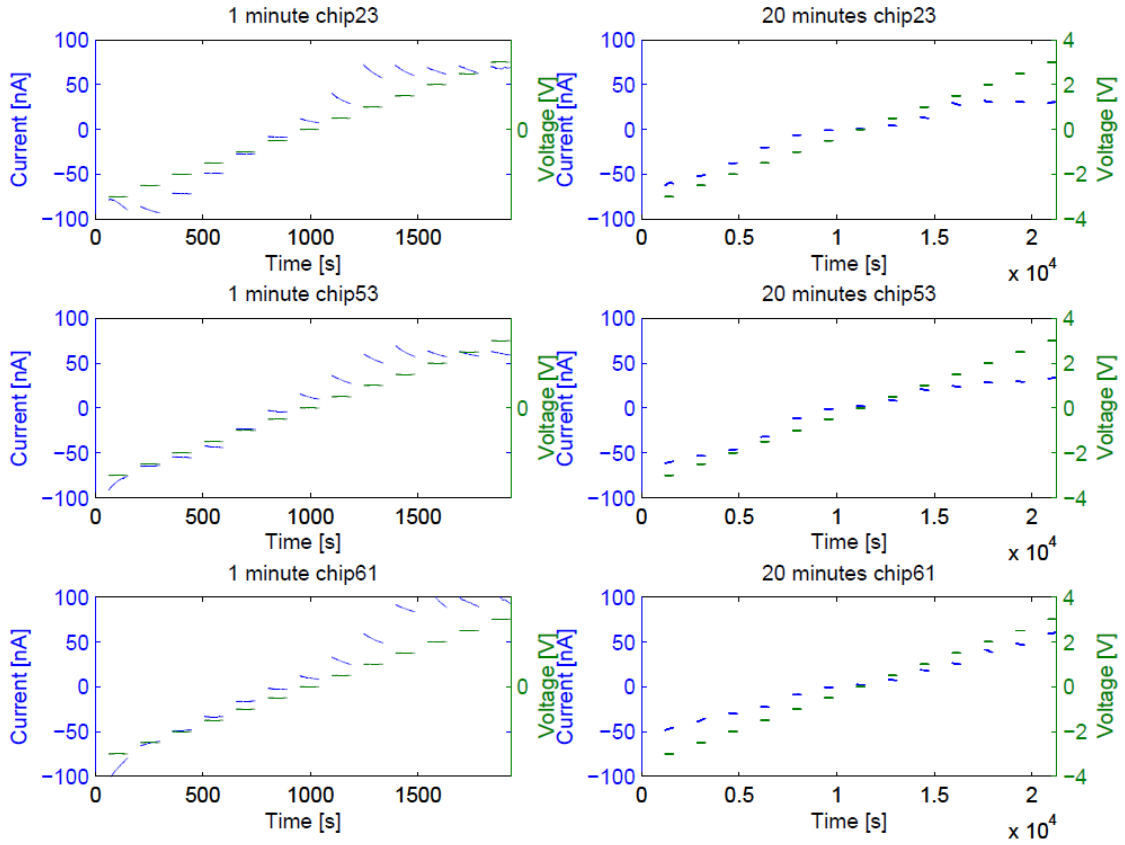

Figure 36: Time dependent dc voltages and currents during a impedance spectroscopy experiment. The voltages and currents are measured during the frequency sweep. The current during the t_{wait} before the sweep is not measured. The bias voltage during t_{wait} equals the voltage during the frequency sweep.

The time constant of the effect that causes the current to decrease is very long. First, there is a waiting time of 1 minute after a bias voltage is applied. The frequency sweep, subsequently, takes another minute and a half. At that moment, the current is still decreasing. By comparing the left and right side of Figure 36, it can be seen that the constant current that is reached after 20 minutes is in some instances only half the current after 2.5 minutes.

The charging of the double layer capacitance of the electrodes does not explain this observation. The double layer capacitance is previously estimated to be around 110nF. The maximum channel impedance seen in Figure 35 is 40MΩ. Multiplying both gives a time constant of τ_{DL}= RC = 4 seconds, which is much shorter than the observed time constant.

Moreover, the depletion of the nanochannels also has a much shorter time constant. A rough estimate of the depletion time can be obtained by calculating how much charge the nanochannels contain when they are filled with a 1mM buffer solution and how large the depletion current is. The amount of charge, q, in the nanochannel is:

$$q = whlC_bF = 10^{-4} \cdot 6 \cdot 10^{-8} \cdot 1.2 \cdot 10^{-4} \cdot 1 \cdot 10^{5} = 7.2 \cdot 10^{-11}C$$

From the left hand side of Figure 36, it can be seen that the effect with a large time constant occurs for currents up to 100nA. The part of the current that is used for depletion can be calculated from the cation to anion ratio α as given in Equation (1.36). If the gold side does not

have any surface charge, than it cation to anion ratio α_{gold}=1. For the glass side α_{glass}=4 is found when a surface charge density of -4.4mC/m^2 is used [3][7]. This value deviates from a surface charge density of -60mC/m^2 used to determine the surface conduction [12]. The origin of the discrepancy between the two values lies in the methods that are used to obtain the surface charge. The value of -60mC/m^2 is found with titration experiments. The lower value of -4.4mC/m^2 is derived from the ζ-potential, which in turn is found from measuring electroosmotic flow. The latter method is used in literature for fluidic diodes and is therefore also used here for the calculation of the cation to anion ratio. A cation to anion ratio of 4 means that at the glass side of the channel, 80% of the current is carried by the cations and 20% by the anions. Consequently, 30% of the current is used to deplete the channel. Multiplying that percentage with the total current of 100nA gives a depletion current of 30nA. The depletion time is than 72pC/30nA=2.4ms. The time constant of the depletion and accumulation of the nanochannels is very fast. Even if it would be overestimated by an order of magnitude, it would not explain the decreasing currents of Figure 36.

5.3.2 Concentration polarization at the micro-nanochannel interface

Up until now, only depletion and accumulation effects inside the nanochannels have been considered. The microchannels and their impedances are considered to be constant. This is not necessarily the case, however. It is possible that the microchannels are depleted of ions due to an effect called concentration polarization. Similar to the nanochannel depletion, it is caused by an asymmetry between the cation to anion ratio. Such a situation is shown in Figure 37. The current in the microchannel is carried equally by cations and anions. In the nanochannel, a larger part of the current is carried by the cations. This asymmetry leads to a depletion of both cations and anions at the interface. The opposite effect occurs at the other end of the channel, where ions accumulate.

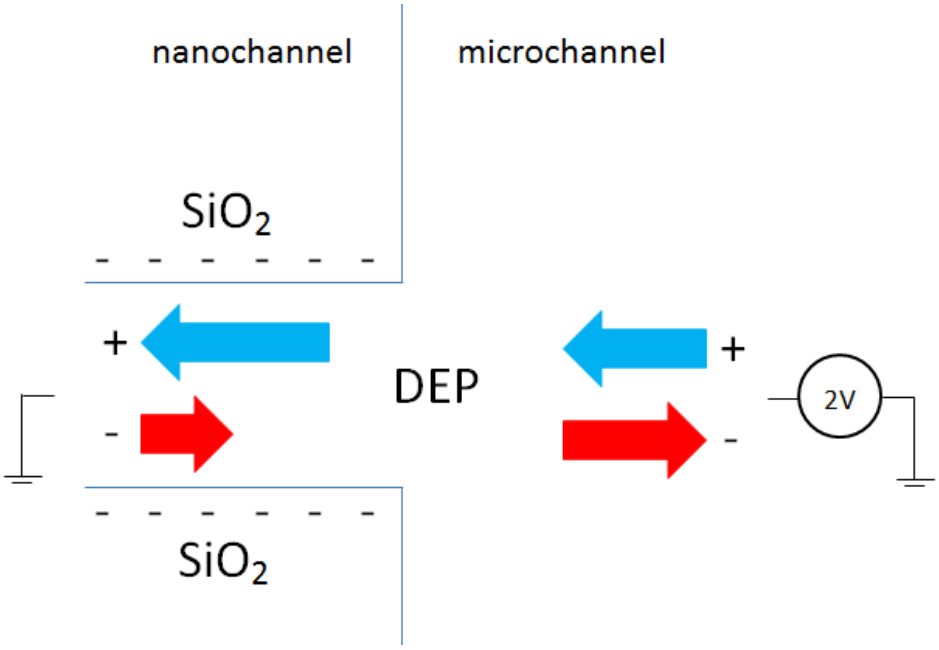

Figure 37: Concentration polarization at the micro- nanochannel interface. In the microchannel, the cations (in blue) and anions (in red) carry equal currents. In the nacochannel, more current is carried by the cations, leading to depletion of both cations and anions.

The resistance of the microchannel where depletion occurs will increase and the resistance of the other channel will decrease. The series resistance is equal to the sum of both, and thus dominated by the largest resistance. Therefore, the microchannel resistance increases due to concentration polarization. If the potential over the system is reversed, the depletion of ions will occur in the other microchannel. The effect will be stronger for larger current. It follows that the voltage dependent impedance due to concentration polarization has the same v-shape as the measurements of Figure 35.

The time constants involved in the depletion of the microchannel are estimated. The approach is similar to the approach of calculating the depletion time of the nanochannel. That is, the current that adds to the depletion is compared to the charge that is present in the volume that is depleted. Initially, the volume of the microchannel that is right in front of the nanochannels is considered. That volume is shown in Figure 38.

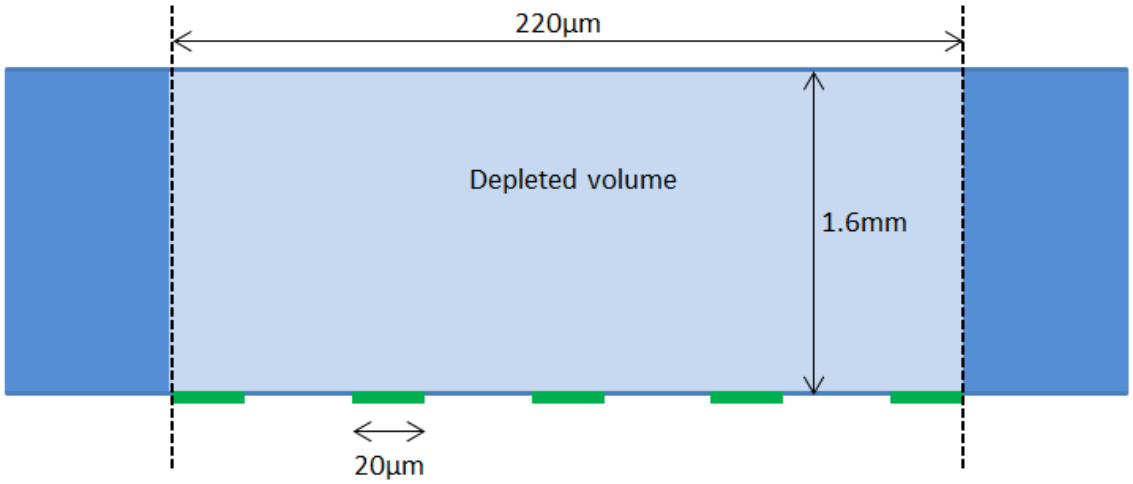

Figure 38: The volume of the microchannel in front of the nanochannels that for which the depletion time due to concentration polarization is calculated so that the time constant of that effect can be estimated.

The depletion current is the same as the depletion current of the nanochannel, which is 30nA. The total charge in the volume is:

$$q = whlC_bF = 2.2 \cdot 10^{-4} \cdot 2 \cdot 10^{-5} \cdot 1.6 \cdot 10^{-3} \cdot 1 \cdot 10^{5} = 7 \cdot 10^{-7} C$$

The time to deplete the volume in front of the nanochannels is than about 23 seconds. This order of magnitude calculation suggests that the depletion is fast enough to influence both the impedance measurement with a t_{wait} of 1 minute as those with a t_{wait} of 20 minutes. This analysis can also be used to calculate the time it would take to deplete the whole channel. The total length of a microchannel is 7mm and it follows that the depletion time would be about 700 seconds. This large time constant might be the reason that the currents at the left side of Figure 36 are still decreasing, while those at the right side are almost constant. It can also explain why there is a difference between the curves of Figure 35. The faster experiment, shown in red, lags behind the slow one, shown in blue, because the depleted microchannels have not reached a steady state yet.

The depleted area of the microchannels has a lower buffer concentration than the bulk concentration at the inlets. Therefore, there is a concentration gradient along the channel which leads to a diffusion current that replenishes the ion depleted region. The maximum steady state current that can flow through the system is limited by that diffusion current. It seems that the currents of chip 23 and 53 in Figure 36 indeed stabilize for increasing positive values.

5.3.3 The effect of a gate potential

The effect of a gate potential on the impedance of the system is examined with the lock-in amplifier. First, experiments without a gate potential are performed so that they can be compared to the results of the experiments with the potentiostat. Figure 39 shows the results for chip 61 with a 1mM solution. The blue lines represent five experiments without bias voltage an the red lines two experiments with a potential difference of -2.8V between the glass side and the gold side. The bias voltage is only applied several minutes before the frequency sweep. All sweeps are carried out sequentially. The duration of one experiment is 2 minutes and the sweep starts with the low frequencies.

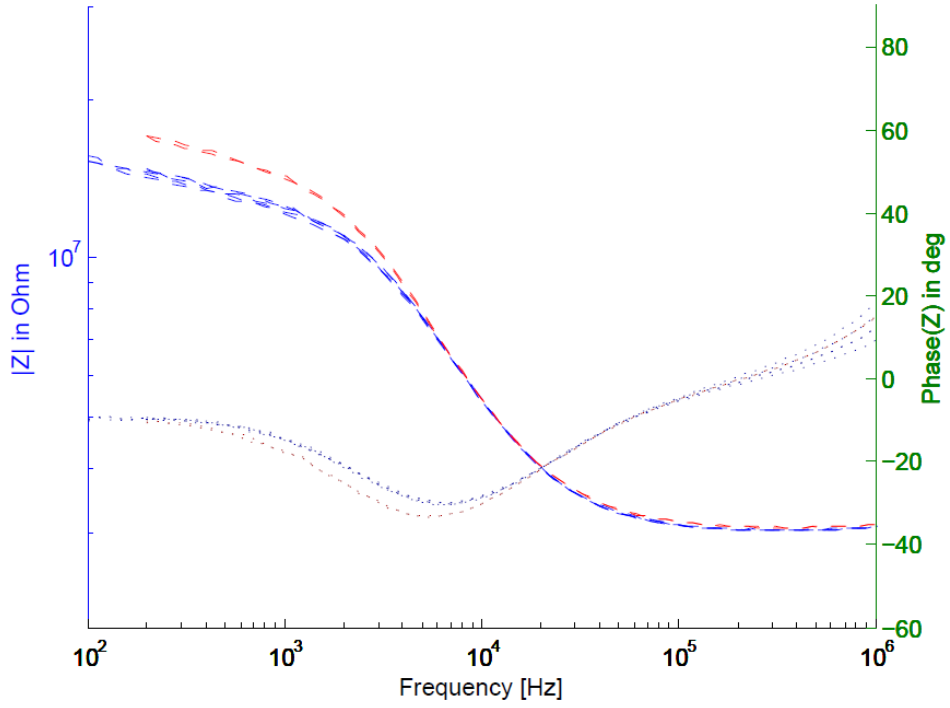

Figure 39: Bode plot of the nanochannel impedance for a 1mM buffer solution and measured with the lock-in amplifier. In red the results when no bias voltage is applied and in blue the results for a bias voltage of -2.8V. The dotted lines are the phase plots and the dashed lines the impedances.

The results of the experiments without a dc bias, shown in blue, are similar in magnitude and phase to the results obtained with the potentiostat as can be seen in Figure 34. The experiments with a bias voltage, shown in red, show a higher impedance, which is consistent with the results obtained with the potentiostat.

Subsequently, a gate voltage is applied over the chip. The flap on chip 61 has an area 2300 times higher than that of the double layer capacitance of the floating gold in the nanochannel. Three experiments are performed with a gate voltage of 1, 2 and 3kV. Moreover, an additional

experiment without a gate voltage is performed in between. The results are given in Figure 40. The positive gate voltage increases the surface charge of the gold. As the glass side is oppositely charged, this enhances the depletion and accumulation capabilities of the diode. The diode is biased in depletion, which means that the impedance should increase. The effect of concentration polarization, however, is expected to be constant or reduced somewhat, as the negative surface charge of the glass walls should be reduced slightly by the gate potential. The results show that the impedance increases. However, the impedance does not increase with increasing gate voltage. It might be that the high gate voltage leaks away or charges other parasitic capacitances.

The additional experiment without a gate voltage is shown in red. Its impedance at low frequencies overlaps with the results of the previous experiments with no gate voltage. At frequencies above 1kHz, however, it deviates from those values and approaches the curves of the experiments with a gate voltage. This difference at high frequencies may be caused by a change in parasitic capacitance due to the addition of a gate and the absence of the chip holder.

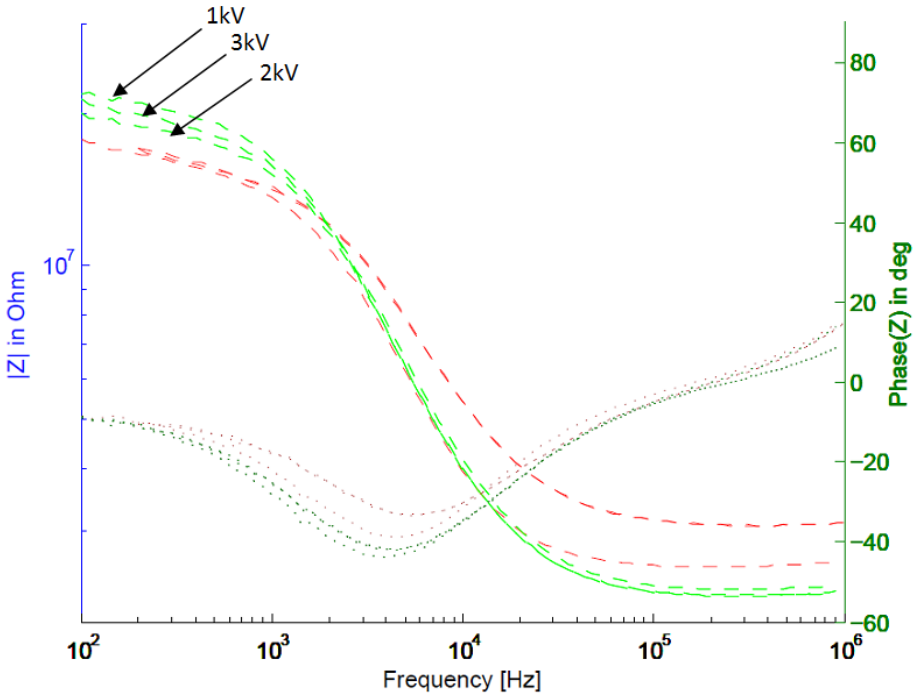

Figure 40: Bode plot of the nanochannel impedance with a voltage bias of -2.8V are shown in red. The results when a gate voltage is applied are shown in green. The dotted lines are the phase plots and the dashed lines the impedances.

6. Conclusions and recommendations

An electroosmotic flow pump in a glass channel with an electrically floating gold surface has been designed and fabricated. It is necessary to split that gold surface into electrically isolated strips to prevent electrolysis. Electrical shorts are observed between these strips, which decrease the voltage that can be applied over the channel before bubbles are formed.

Large gold flaps that are used to enhance to capacitive control of the surface charge, however, the flaps create bonding issues so that the solution leaks out of the microchannel. Consequently, the double layer capacitance of the flaps is increased. No influence of a gate voltages is observed. This absence is caused by to the increased double layer capacitance due to the leaks and the relatively small overlap are between the flaps and the gate electrode.

Electroosmotic flow is observed with particle tracking velocimetry. However, the low hydrodynamic resistance of the channel causes an undesired influence of pressure driven flow and makes the measurement very delicate.

A nanofluidic channel with a glass-gold junction is designed and fabricated. A theory is derived that predicts that the junction will deplete of ions independent of the direction of the current. This behavior deviates from the diodes previously described in literature and is caused by the polarization of the gold surface in the presence of an electric field. Such behavior is also found experimentally. However, an analysis of the time constant of the process indicates that this effect is caused by a depletion of the microchannel. This phenomenon obscures the behavior of the nanochannels and the derived theory can therefore not be verified.

The application of a positive potential on the gate of the fluidic diode increased the impedance of the system slightly. This corresponds to the diode theory that predicts that the gate voltage enhances the depletion of the nanochannels. On the contrary, it cannot be attributed to microchannel depletion, indicating that the originates in the nanochannels. The impedance did not increase, however, with a further increase in gate potential, which indicates that there are still unknown current leaks or parasitic capacitances that influence the system.

A major problem of the electroosmotic flow pump is a pressure driven flow due the low hydrodynamic resistance of the microchannel. That resistance can be greatly increased by lowering the height of the channel. Alternatively, the channel length could be increased.

Both the pump and the diode suffer from fluidic leaks due to the poor bonding of gold to glass. This problem might be solved by adding an additional adhesion layer on top of the gold flaps. Reducing the leaks between the microchannels of the diode is expected to greatly reduce the electric current between them, due to the absence of surface conduction parallel to the nanochannels. The depletion effects in the microchannels would simultaneously be reduced. That depletion can be removed entirely by creating a constant flow through the microchannels and continuously replacing any depletion or accumulation of ions.

The voltage control can be further optimized so that the necessary gate voltage can be decreased. The largest part of the area of the flap in the current rectifier is already located at a large distance of the fluidic channels. A hole could be powderblasted in the top wafer before bonding with the same dimensions as that flap. After bonding, a thin, electrically isolating layer

can be applied to cover the bare gold flap. This layer can be made much thinner than the currently used 500µm, thereby lowering the necessary gate voltage. A similar approach can be taken for the microfluidic pumps. These systems, however, have a larger gold surface inside the channel and therefor a larger double layer capacitance, which makes capacitive control of the surface charge more difficult.

7. Bibliography

[1] "Critical Thinking," *realkato.com*, 2007. [Online]. Available: http://www.realkato.com/blog.php?pid=857.

[2] R. Schasfoort, S. Schlautmann, J. Hendrikse, and van den Berg A, "Field-effect flow control for microfabricated fluidic networks," *Science (New York, N.Y.)*, vol. 286, no. 5441, pp. 942–5, Oct. 1999.

[3] W. Guan, R. Fan, and M. a Reed, "Field-effect reconfigurable nanofluidic ionic diodes.," *Nature communications*, vol. 2, p. 506, Jan. 2011.

[4] R. B. H. Veenhuis, E. J. van der Wouden, J. W. van Nieuwkasteele, A. van den Berg, and J. C. T. Eijkel, "Field-effect based attomole titrations in nanoconfinement.," *Lab on a chip*, vol. 9, no. 24, pp. 3472–80, Dec. 2009.

[5] A. J. Bard, L. R. Faulkner, E. Swain, and C. Robey, *Fundamentals and Applications*, 2nd ed. .

[6] R. Karnik, C. Duan, K. Castelino, H. Daiguji, and A. Majumdar, "Rectification of ionic current in a nanofluidic diode.," *Nano letters*, vol. 7, no. 3, pp. 547–51, Mar. 2007.

[7] L.-J. Cheng and L. J. Guo, "Ionic current rectification, breakdown, and switching in heterogeneous oxide nanofluidic devices.," *ACS nano*, vol. 3, no. 3, pp. 575–84, Mar. 2009.

[8] I. Vlassiouk and Z. S. Siwy, "Nanofluidic diode.," *Nano letters*, vol. 7, no. 3, pp. 552–6, Mar. 2007.

[9] L.-J. Cheng and L. J. Guo, "Nanofluidic diodes.," *Chemical Society reviews*, vol. 39, no. 3, pp. 923–38, Mar. 2010.

[10] E. Bogatin, "Design Rules for Microstrip Capacitance," *IEEE Transactions on Components, Hybrids, and Manufacturing Technology*, vol. 11, no. 3, pp. 253–259, Sep. 1988.

[11] T. M. Squires and M. Z. Bazant, "Induced-charge electro-osmosis," *Journal of Fluid Mechanics*, vol. 509, pp. 217–252, Jun. 2004.

[12] D. Stein, M. Kruithof, and C. Dekker, "Surface-Charge-Governed Ion Transport in Nanofluidic Channels," *Physical Review Letters*, vol. 93, no. 3, pp. 1–4, Jul. 2004.

[13] L. Cademartiri and G. Ozin, *Concepts of nanochemistry*. Weinheim: Wiley-VCH, 2009.

[14] *Handbook of Chemistry and Physics*, 83rd Editi. CRC press.